Appendix 3.1 Benchmark cases for EZ Frisk and OpenQuake

L. Fülöp, Marianne Malm, Espoo, 18.02.2019

Issue raised by expert group:
PEER test the software used.

Suggested resolution by expert group
NA

Comments

1. Introduction

We benchmark the two PSHA software used in SENSEI against an established calculation example (Thomas et al, 2016). We specifically choose an example with areal seismic source zones for the test. The description is as follows:

"***Case 10*** –

Purpose: Area source with fixed depth of 5km. Calculate the hazard at four sites for the area source defined in Figure 3.1. Use the truncated exponential model with Mmax = 6.5 and Mmin=5.0. Source should be uniformly distributed point sources (or approximations to point source) across the area (1 km grid spacing) at a fixed depth of 5 km. The attenuation relationship is Sadigh et al. (1997), rock, sigma =0.

Results: Test Case 10 tests the computation of hazard from an area source. The case was defined as having uniformly distributed point sources throughout the area at a fixed depth. However, some of the codes tested do not implement point sources. These codes used an area source defined with uniformly distributed small faults that were set to be 1 square km in size. Even with these differences, results from all codes are consistent, as shown in Figures 3.98–3.101."

Figure 3.1 from the quoted text above is reproduced in Figure 1a below; and results from Figures 3.98–3.101 in Figure 1b for the Sites 1 and 4.

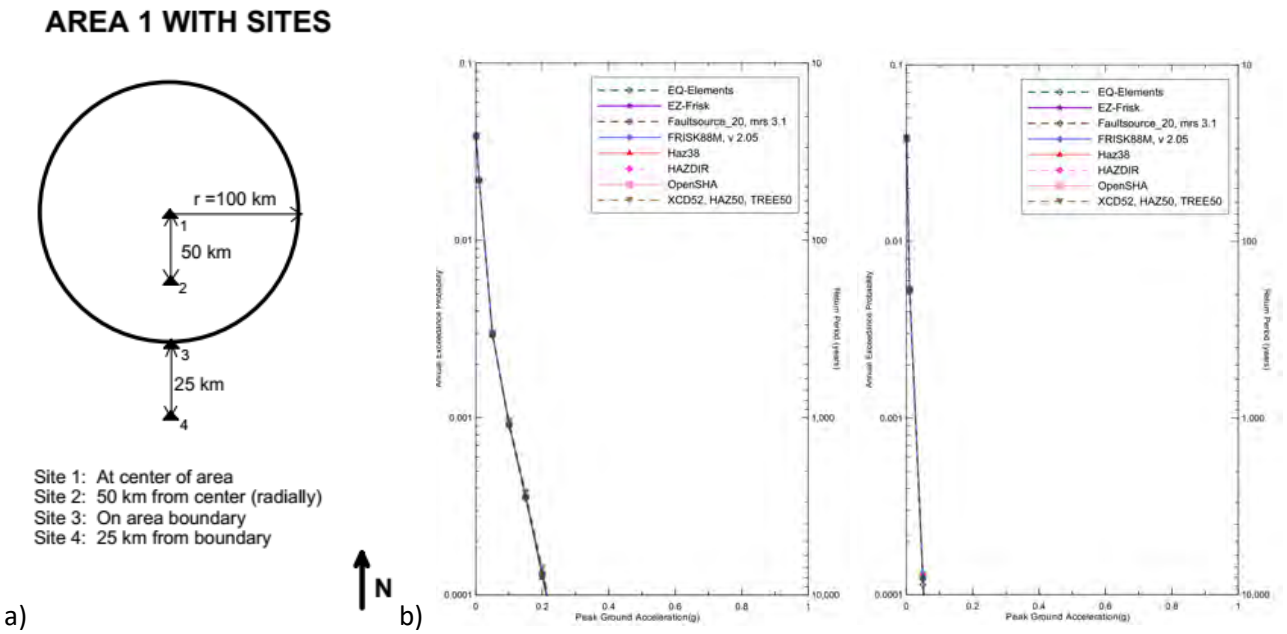

Figure 1: *Areal source of the benchmark case with results for Site#1 and Site#4.*

2. Test cases

The coordinates of the benchmark case, in the PEER report, define a circular area located in California. It was not possible to run the case with EZFrisk due to license limitation. Hence,

- Step 1: The original benchmark case was run with OpenQuake. It was confirmed that the OpenQuake model reproduces the original results from Figure 1b.
- Step2: an identical circular source area was established in Finland with identically placed sites relative to the source area (Figure 2b). The coordinates translated to Finland are given in Annex A. For this case the calculation was repeated with OpenQuake; and it was established that the results are quasi-identical to the initial (Californian results)
- Step 3: The sigma of the Sadigh et al. (1997) GMPE was not truncated to 0, as in the initial benchmarks. Instead, the run was with non-truncated sigma (Obs. For numerical stability truncation of 6 was used in OpenQuake, which approximates non-truncated). The result of Step 3 is the first that can be obtained with both with OpenQuake and EZ Frisk.
- Step 4: The GMPE was swapped for the FennoG16 and the NGA-East weighted average table implementation, which we used in the runs of SENSEI. This GMPE's were also used un-truncated.

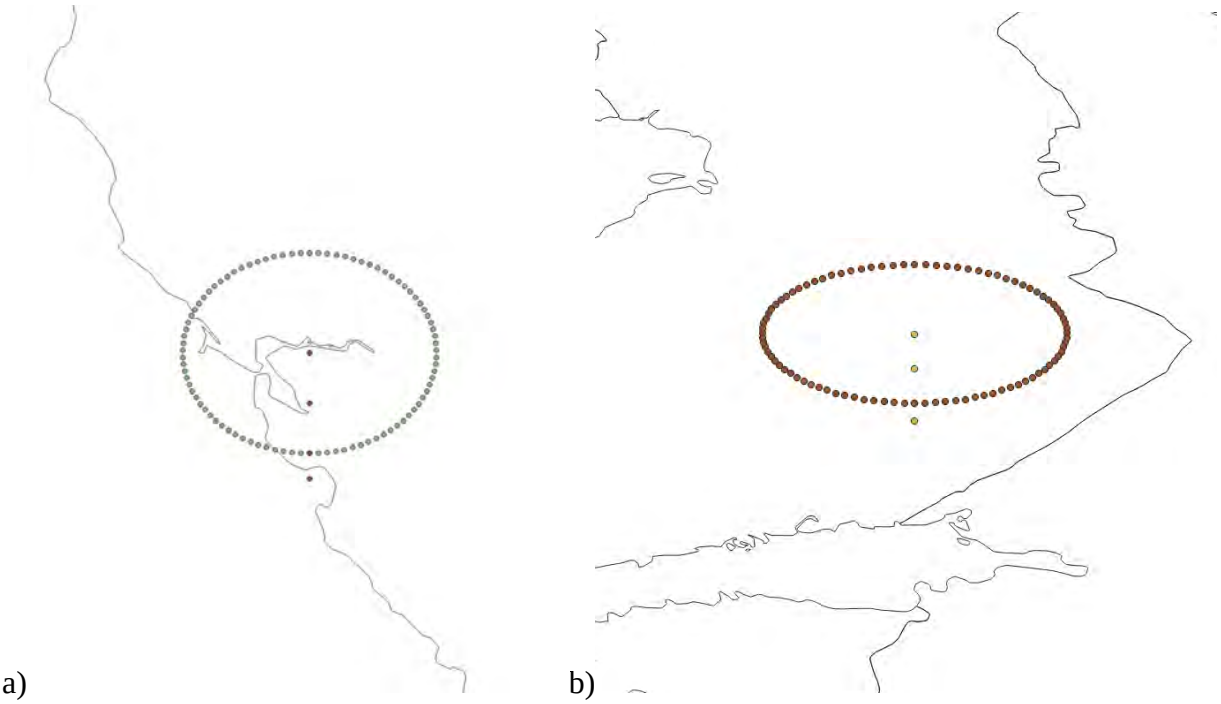

a) b)

Figure 2: *Areal source of the benchmark case displayed with (a) centre in California and (b) in Finland. The oval representation of the circle in Finland's case is due to projection.*

3. Results

In STEP1 and STEP2, we confirm that the OpenQuake model replicates the PEER vales for the base model both in California and with the translated circular SSA in Finland (Table 1).

Table 1: *Step1 and Step2 of the benchmarking calculation demonstrate that the OpenQuake engine reproduces the PEER results both with the circular SSA localized in California and Finland*

	PEER reference values		**OpenQuake model in California (SSA in Figure 2a)**		**OpenQuake model in Finland (SSA in Figure 2b)**	
GMPE	Sadigh et al. (1997)		Sadigh et al. (1997)		Sadigh et al. (1997)	
σ truncation	0		0		0	
PGA(g)	**Site#1**	**Site#4**	**Site#1**	**Site#4**	**Site#1**	**Site#4**
0.001	3.87E-02	3.83E-02	3.88E-02	3.83E-02	3.88E-02	3.83E-02
0.01	2.19E-02	5.33E-03	2.19E-02	5.41E-03	2.20E-02	5.37E-03
0.05	2.97E-03	1.25E-04	2.99E-03	1.33E-04	3.00E-03	1.18E-04
0.1	9.22E-04	1.63E-06	9.28E-04	2.27E-06	9.34E-04	1.34E-06
0.15	3.59E-04		3.62E-04		3.65E-04	
0.2	1.31E-04		1.34E-04		1.35E-04	
0.25	4.76E-05		4.83E-05		4.85E-05	
0.3	1.72E-05		1.76E-05		1.77E-05	
0.35	5.38E-06		5.75E-06		5.95E-06	
0.4	1.18E-06		1.37E-06		1.38E-06	

STEP 3 explores the effect of truncation. As expected, the sigma truncation severely reduced the hazard in the earlier models, and the increase is now observed in Table 3. Table 3 also compares the values obtained

in OpenQuake with those from EZFrisk. We were able not able to use EZFrisk in the earlier models due to licensing limitations (i.e., license is regional, and we only have North Europe license; the tampering with the default GMPE sigma in EZFrisk is not trivial).

Table 2: *Step3*

	OpenQuake model in Finland (SSA in Figure 2b)		**EZ Frisk model in Finland (SSA in Figure 2b)**	
GMPE	Sadigh et al. (1997)		Sadigh et al. (1997)	
σ truncation	6		no truncation	
PGA(g)	**Site#1**	**Site#4**	**Site#1**	**Site#4**
0.001	3.87E-02	3.51E-02	3.94E-02	3.56E-02
0.01	2.29E-02	6.84E-03	2.31E-02	6.83E-03
0.05	4.11E-03	4.54E-04	4.09E-03	4.53E-04
0.1	1.47E-03	6.55E-05	1.46E-03	6.56E-05
0.15	7.21E-04	1.47E-05	7.15E-04	1.48E-05
0.2	4.03E-04	4.14E-06	4.00E-04	4.20E-06
0.25	2.43E-04	1.36E-06	2.41E-04	1.39E-06
0.3	1.54E-04	5.03E-07	1.53E-04	5.17E-07
0.35	1.01E-04	2.03E-07	1.00E-04	2.10E-07
0.4	6.83E-05	8.80E-08	6.76E-05	9.19E-08

Finally in STEP 4 contains the results for the swapped GMPE's

Table 2: *Step4*

	OpenQuake model in Finland (SSA in Figure 2b)		**OpenQuake model in Finland (SSA in Figure 2b)**		**EZ Frisk model in Finland (SSA in Figure 2b)**		**EZ Frisk model in Finland (SSA in Figure 2b)**	
GMPE	**FennoG16**		**NGAeast-WA**		**FennoG16**		**NGAeast-WA**	
σ truncation	6		6		no truncation		no truncation	
PGA(g)	**Site#1**	**Site#4**	**Site#1**	**Site#4**	**Site#1**	**Site#4**	**Site#1**	**Site#4**
0.001	3.91E-02	3.88E-02	3.91E-02	3.88E-02	3.95E-02	3.91E-02	3.95E-02	3.92E-02
0.01	3.52E-02	2.26E-02	3.18E-02	1.82E-02	3.50E-02	2.15E-02	3.16E-02	1.78E-02
0.05	1.50E-02	4.56E-03	8.56E-03	1.75E-03	1.41E-02	4.19E-03	8.09E-03	1.69E-03
0.1	7.11E-03	1.48E-03	3.34E-03	3.09E-04	6.47E-03	1.36E-03	3.10E-03	3.22E-04
0.15	4.10E-03	6.58E-04	1.82E-03	8.53E-05	3.66E-03	6.11E-04	1.69E-03	9.74E-05
0.2	2.63E-03	3.45E-04	1.16E-03	2.93E-05	2.32E-03	3.23E-04	1.07E-03	3.67E-05
0.25	1.81E-03	2.00E-04	7.99E-04	1.15E-05	1.58E-03	1.89E-04	7.33E-04	1.58E-05
0.3	1.30E-03	1.24E-04	5.79E-04	4.99E-06	1.13E-03	1.18E-04	5.28E-04	7.40E-06
0.35	9.70E-04	8.13E-05	4.33E-04	2.31E-06	8.32E-04	7.78E-05	3.93E-04	3.71E-06
0.4	7.42E-04	5.53E-05	3.33E-04	1.13E-06	6.32E-04	5.33E-05	2.99E-04	1.96E-06

4. Conclusions

References

Thomas, P., Wong I., Abrahamson N., 2016, Verification of Probabilistic Seismic Hazard Analysis Computer Programs, PEER Report 2010/106

Sadigh, K., Chang, C.-Y., Egan, J.A., Makdisi, F., Youngs, R.R., 1997. Attenuation Relationships for Shallow Crustal Earthquakes Based on California Strong Motion Data. Seismological Research Letters 68, 180–189. https://doi.org/10.1785/gssrl.68.1.180

Appendix A:

	Circular SSA in California			Circular SSA in Finland	
Center	-122	38		28	63
Site #1	-122	38		28	63
Site #4	-122	36.874		28	61.874
Radius:	100 km			100 km	

Circular SSA in California			Circular SSA in Finland	
Coordinates			Coordinates	
-123.138	38.026		27.602	62.122
-123.137	37.963		27.472	62.137
-123.134	38.089		27.344	62.155
-123.131	37.9		27.219	62.178
-123.124	38.151		27.098	62.205
-123.119	37.838		26.981	62.235
-123.108	38.213		26.868	62.27
-123.101	37.777		26.761	62.307
-123.087	38.273		26.659	62.348
-123.079	37.717		26.563	62.392
-123.06	38.333		26.474	62.439
-123.051	37.658		26.392	62.489
-123.029	38.39		26.317	62.541
-123.018	37.601		26.25	62.596
-122.992	38.446		26.192	62.652
-122.98	37.545		26.141	62.71
-122.95	38.5		26.1	62.77
-122.937	37.492		26.067	62.831
-122.904	38.551		26.044	62.893
-122.89	37.442		26.03	62.955
-122.853	38.6		26.026	63.018
-122.839	37.394		26.032	63.08
-122.798	38.645		26.047	63.142
-122.784	37.349		26.071	63.204
-122.739	38.688		26.106	63.265
-122.725	37.308		26.149	63.324
-122.676	38.727		26.203	63.382
-122.663	37.269		26.265	63.438
-122.61	38.762		26.336	63.492
-122.597	37.234		26.415	63.544
-122.54	38.794		26.503	63.593
-122.529	37.203		26.598	63.639

-122.468	38.822		26.701	63.681
-122.458	37.176		26.811	63.721
-122.394	38.846		26.926	63.757
-122.385	37.153		27.048	63.789
-122.318	38.866		27.174	63.817
-122.31	37.133		27.305	63.841
-122.24	38.881		27.439	63.861
-122.234	37.118		27.577	63.877
-122.16	38.892		27.717	63.888
-122.157	37.108		27.858	63.895
-122.08	38.899		28	63.897
-122.078	37.101		28.142	63.895
-122	37.099		28.283	63.888
-122	38.901		28.423	63.877
-121.922	37.101		28.561	63.861
-121.92	38.899		28.695	63.841
-121.843	37.108		28.826	63.817
-121.84	38.892		28.952	63.789
-121.766	37.118		29.074	63.757
-121.76	38.881		29.189	63.721
-121.69	37.133		29.299	63.681
-121.682	38.866		29.402	63.639
-121.615	37.153		29.497	63.593
-121.606	38.846		29.585	63.544
-121.542	37.176		29.664	63.492
-121.532	38.822		29.735	63.438
-121.471	37.203		29.797	63.382
-121.46	38.794		29.851	63.324
-121.403	37.234		29.894	63.265
-121.39	38.762		29.929	63.204
-121.337	37.269		29.953	63.142
-121.324	38.727		29.968	63.08
-121.275	37.308		29.974	63.018
-121.261	38.688		29.97	62.955
-121.216	37.349		29.956	62.893
-121.202	38.645		29.933	62.831
-121.161	37.394		29.9	62.77
-121.147	38.6		29.859	62.71
-121.11	37.442		29.808	62.652
-121.096	38.551		29.75	62.596
-121.063	37.492		29.683	62.541
-121.05	38.5		29.608	62.489
-121.02	37.545		29.526	62.439

-121.008	38.446		29.437	62.392
-120.982	37.601		29.341	62.348
-120.971	38.39		29.239	62.307
-120.949	37.658		29.132	62.27
-120.94	38.333		29.019	62.235
-120.921	37.717		28.902	62.205
-120.913	38.273		28.781	62.178
-120.899	37.777		28.656	62.155
-120.892	38.213		28.528	62.137
-120.881	37.838		28.398	62.122
-120.876	38.151		28.267	62.111
-120.869	37.9		28.134	62.105
-120.866	38.089		28	62.103
-120.863	37.963		27.866	62.105
-120.862	38.026		27.733	62.111

Appendix 3.2

Appendix 3.2 On seismic source areas in the Fennoscandian Shield, with focus on the Loviisa NPP

P. Mäntyniemi, M. Malm, L. Rinne, L. Fülöp 13 Feb 2020

Issue raised by the expert group: **Line 33 in the SENSEI excel table**

Uniform versus variable seismicity within source zones

Suggested solution by the expert group

It is commonly assumed that the seismicity rate per unit area in a source zone is constant. This assumption may or may not be appropriate, depending on the spatial uniformity of the seismicity. This issue may be particularly important for the source zones containing the site or very near the site. Musson (2000) provides a nearest-neighbor simulation procedure to test the validity of this assumption.

Introduction

In the absence of mapped active faults and other identified seismogenic structures, seismic area sources are typically designed in a given target region for probabilistic seismic hazard analysis (PSHA). The area sources assume the shapes of polygons, and are taken to represent homogeneous seismicity in terms of earthquake activity rates and frequency-magnitude distributions (Pagani et al. 2010). Moreover, they should belong to the same seismotectonic regime.

Defining seismic area sources with homogeneous seismicity in the Fennoscandian Shield is intriguing, because seismicity maps there show areas of enhanced seismicity. This feature has been recognized in onshore areas for a long time: earthquake occurrence probabilities are not constant over the whole region. Therefore discerning seismic area sources visually, or by other means, on the basis of the spatial distribution of observed seismicity is rather appealing. A complication is that nuclear power plants (NPP) are located in areas of low and diffuse seismicity, so there may be a difference of judgment into the best approach to designing the host source area and neighbouring areas for these sites. This document especially focuses on the Loviisa NPP in southern Finland.

Seismic area source no. 10

The area composed of Wiborg rapakivi granite in S-SE Finland was designed as a separate seismic area source in all three source area models presented by Korja and Kosonen (2015). The rapakivi granite is composed of lighter material than the surrounding bedrock, and is also much younger, ~1.65 Ga old. Their main argument for a separate rapakivi area was the unusual seismicity of shallow earthquake swarms. They also commented that there are no lineaments in this area. The southern boundary followed from the 500-km radius from the target site of the 2015 PSHA (Korja and Kosonen 2015 p. 180). The three rapakivi source areas (nos. 1.14, 2.12, 3.21) in their models are very similar.

Korja et al. (2018) designed the seismic area source (no. 10) composed of the Wiborg rapakivi granite (Fig. 1). It is larger than the previous rapakivi area sources and covers larger portions of the Gulf of Finland and the Russian territory to the SE-E. It is the host area of the Loviisa NPP.

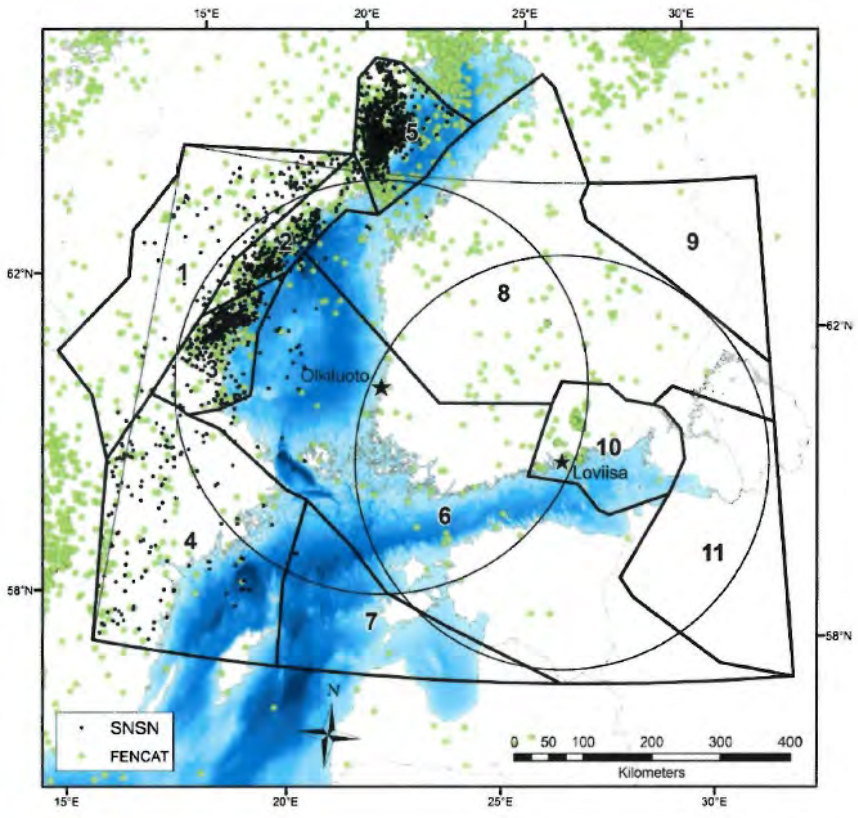

Figure 1. *Seismic area sources 1 to 11: the main division. The two circles with a 300-km radius encircle the NPP sites Olkiluoto and Loviisa denoted by stars. From Korja et al. (2018)*

As pointed out by the expert group and G. Toro in particular at the beginning of the SENSEI project, the observed seismicity appears to be confined to the western portion of area source no. 10; it is uniform geologically rather than seismically, in spite of the original intent. Whether this is a real seismicity feature is an open question. Some comments are included at the end of this document.

It is a useful exercise to test the effect of different boundaries around the recorded seismicity. The design in Figure 1 was modified in two steps (Fig. 2), which diminished the size of area source no. 10 and increased that of no. 6 (Table 1). The smallest version of area source no. 10 is approximately one third of the largest one. No other area sources were included in the computations. The intent was to monitor the effect on the output, not to aim at final seismic hazard results.

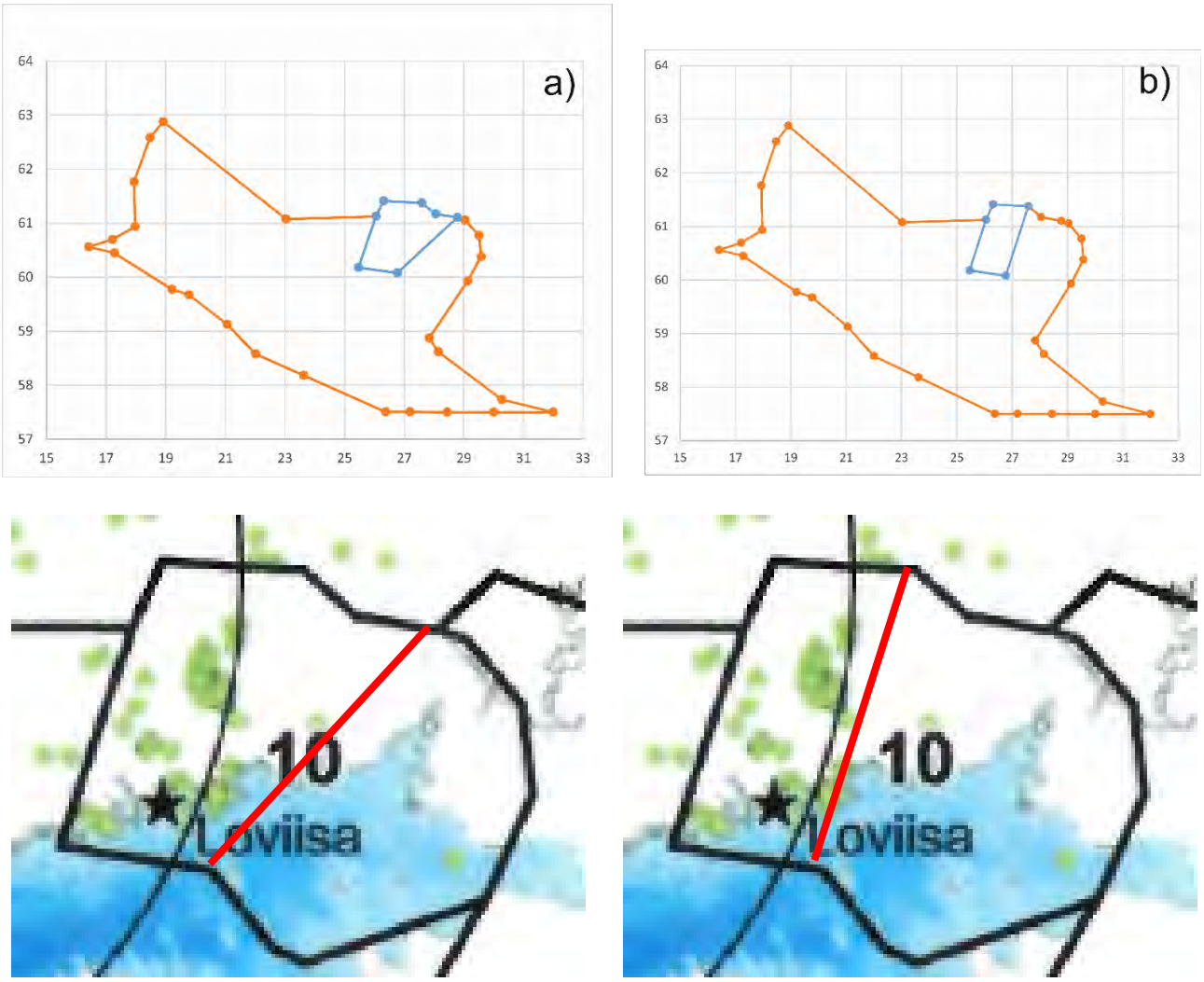

Figure 2. *a)b) Two alternative designs of the seismic area source no. 6 (orange line) and no. 10 (blue line). The lower part shows the available earthquake epicenters (green dots) and the divisions of area source no. 10 by red lines. The star denotes the NPP site.*

Table1. Sizes of the different designs of the seismic area sources (in km^2).

Area source boundaries	Area no. 6	Area no. 10
As in Figure 1	190991.0	29446.9
2a	205151.2	15300.8
2b	210089.1	10366.9

The swarms are typically located in the uppermost 2 km of the crust. The depth range used was 0-10 km, because Elo and Korja (1993) suggested that the rapakivi granite extends down to the depth of 10 km at least. The same depth range was also used for area no. 6, although it is a large area that exhibits seismicity over a wider depth range. The few depth determinations available for its eastern part are shallow, though. The main point is that only one and the same depth range (and other input) is used for the three area source designs. Different depth alternatives shall be incorporated in the final logic tree for both area sources.

Excluding the easternmost swarm located to the east of the pronounced concentration of epicentres in the west of the area source has no effect on the input parameters β and λ (Table 2). The NGA-East weighted mean ground-motion prediction equation (GMPE) was used in the test.

Table 2. Input parameters for the two seismic area sources.

Area	beta	lambda	depth range (km)	M_{min}	M_{max}
No. 6	2.57	0.003296649	0-10	4	6.5
No. 10	2.46	0.00058064	0-10	4	6.5

Tables 3-6 show the output in terms of acceleration values for PGA (Table 3), 25 Hz (Table 4), 5 Hz (Table 5), and 1 Hz (Table 6) for annual frequencies of exceedance (AFE) from 10^{-3} to 10^{-7}.

Table 3. PGA in units of g (NGA-East weighted mean GMPE)

Area source boundaries	AFE 10^{-3}	AFE 10^{-4}	AFE 10^{-5}	AFE 10^{-6}	AFE 10^{-7}
As in Figure 1	0.002045	0.01805	0.09556	0.3317	0.8028
-“- 2a	0.002469	0.02661	0.1388	0.4397	0.9839
-“- 2b	0.002736	0.03455	0.1739	0.5139	1.090

Table 4. Spectral acceleration at 25 Hz in units of g (NGA-East weighted mean GMPE)

Area source boundaries	**AFE 10^{-3}**	**AFE 10^{-4}**	**AFE 10^{-5}**	**AFE 10^{-6}**	**AFE 10^{-7}**
As in Figure 1	0.004523	0.04212	0.2222	0.7597	1.780
-“- 2a	0.005606	0.06286	0.3277	1.001	2.188
-“- 2b	0.006240	0.08200	0.4076	1.146	2.441

Table 5. Spectral acceleration at 5 Hz in units of g (NGA-East weighted mean GMPE)

Area source boundaries	**AFE 10^{-3}**	**AFE 10^{-4}**	**AFE 10^{-5}**	**AFE 10^{-6}**	**AFE 10^{-7}**
As in Figure 1	0.002712	0.02013	0.08847	0.2915	0.7321
-“- 2a	0.003151	0.02655	0.1217	0.3891	0.9072
-“- 2b	0.003408	0.03219	0.1485	0.4568	1.019

Table 6. Spectral acceleration at 1 Hz in units of g (NGA-East weighted mean GMPE)

Area source boundaries	**AFE 10^{-3}**	**AFE 10^{-4}**	**AFE 10^{-5}**	**AFE 10^{-6}**	**AFE 10^{-7}**
As in Figure 1	0.0002468	0.002715	0.01363	0.04577	0.1262
-“- 2a	0.0002823	0.003263	0.01716	0.06111	0.1618
-“- 2b	0.0003055	0.003694	0.02018	0.07295	0.1878

It can be noticed that diminishing the size of the host area increases the acceleration values. Table 7 shows the ratios of acceleration for designs 2b and 1.

Table 7. Ratios of accelerations for designs 2b and 1.

	AFE 10^{-3}	**AFE 10^{-4}**	**AFE 10^{-5}**	**AFE 10^{-6}**	**AFE 10^{-7}**
PGA	1.34	1.91	1.82	1.55	1.36
25 Hz	1.38	1.94	1.83	1.51	1.37
5 Hz	1.26	1.60	1.68	1.57	1.39
1 Hz	1.23	1.36	1.48	1.59	1.49

The largest ratios are observed for AFE 10^{-4} at PGA and 25 Hz, the second largest for AFE 10^{-5} at the same frequencies. AFEs 10^{-3} and 10^{-7} have the smallest ratios, but the increase of the acceleration

value with diminishing source size is clear in these cases as well. Thus the size of the area sources clearly has an impact on the output.

Table 8 shows the same ratios for designs 2a and 1. The input values differed from those used above: the depth range 0-35 km, M_{max} = 5.5 and the original, small M_{min} values, and the VNS2017 GMPE were used. A similar trend is noticed also for this entirely different set of input parameters: The largest ratio is observed for AFE 10^{-4}, the second largest for AFE 10^{-5}, while the smallest ratio is associated with AFE 10^{-7}. AFE 10^{-3} is not available here. The absolute values of the ratios are smaller than those related to Table 3, though.

Table 8. Ratios of accelerations for designs 2a and 1 for the input values described above and from Table 3.

AFE	**(PGA_{new}/PGA_{old})**	**(PGA_{new}/PGA_{old}) from Table 3**
10^{-4}	1.33	1.47
10^{-5}	1.30	1.45
10^{-6}	1.24	1.30
10^{-7}	1.18	1.23

Tests for seismic source zones

Musson (2000) raised the justifiable issue of post-design testing of seismic source zones. He suggested to test the randomness/uniformity of the spatial distribution of epicentres in the area source. According to this approach, assuming the Poisson distribution, the expected mean distance, d_{exp}, between nearest point neighbours is

$$d_{exp} = 0.5 \cdot \sqrt{A/n}, \quad (1)$$

where A is the size of the area and n is the number of points in the area.

The test was run for a smaller data set than that illustrated in Figure 2: twelve epicenters collected between 1985 and 1989 by former utility Imatran Voima were removed since these earthquakes were not recorded by the national network.

Table 9 shows the observed (d_{obs}) and expected (d_{exp}) mean nearest neighbour distances for the three versions of area source no. 10. Their ratio is the nearest-neighbour statistic, *R*. At value 0, it indicates complete clustering at a single point, and at value 1.0 and above total randomness. The maximum value it can obtain, 2.15, indicates a uniform pattern arranged on an equidistant hexagonal matrix. As seen in Figure 2, diminishing the size of the area leaves out only the two longest distances between the nearest points, and this affects the observed mean. The diminishing R value is interpreted to mean that clustering increases as the longest distances between nearest points are removed.

Table 9. Statistical analysis of the three designs of area source no. 10.

Area	**Size (km^2)**	***n***	***d_{obs}* (km)**	***d_{exp}* (km)**	***R* = d_{obs}/d_{exp}**	***s***	***Z***
1	29446.9	33	7.89	14.94	0.53	1.36	5.18
2a	15300.8	32	5.26	10.93	0.48	1.01	5.61
2b	10366.9	31	4.29	9.14	0.47	0.86	5.65

The sampling variance, v, can be written as

$$v = (4 - \pi) \cdot A/(4 \cdot \pi \cdot n^2). \quad (2)$$

Thus the standard error, *s*, of the mean distance becomes

$$s = 0.26136 \cdot \sqrt{A/n^2}. \quad (3)$$

The above *s* can be used in a standard *Z* test to determine the significance of the deviation of the mean nearest neighbour distance from what would be expected for a random pattern of the same density. Table 9 shows the values of the *Z* statistics in the three cases. The statistical significance is >99.99%, indicating significant clustering. According to Musson (2000), either some justifying argument must be produced as to why the clustering should be allowed on tectonic grounds, or it should be modified. –The word “swarm” is used here. However, a largest magnitude, or a few largest magnitudes, can typically be discerned in the swarms, so they can also be understood as prolonged aftershock sequences. This challenges the capability of declustering algorithms to deal with very low-magnitude events.

Below the other arguments by Musson (2000) are commented from the local perspective:

a) comparison with experience

Extending seismic histories far back in time (longer than the time span of the available regional catalogue) is not very realistic. Seismic histories for localities in northern Europe (such as Tornio, Vaasa, and Pyhäjoki on the eastern coast of the Gulf of Bothnia) typically span over two to three centuries, similar to the Fennoscandian earthquake catalogue. They are compact illustrations of the level of earthquake effects at relatively short return periods. Macroseismic intensities and peak ground accelerations are very disparate quantities, however, and it is difficult to estimate the level of ground shaking needed to cause the documented minor damages (e.g. Mäntyniemi and Wahlström 2013).

b) argument from sensitivity

Alternative choices can at times be shown not to have any effect on PSHA results. For example, it is often observed that the site-specific seismic hazard result at plate interiors is dominated by the host source zone and possibly also a contiguous source zone (e.g. Bommer et al., 2013). This is also observed in the Fennoscandian Shield. However, the IAEA (2010) regulation points out that, in plate interiors, it may be necessary to compile earthquake data for more distant sources beyond the boudaries of the target region. This probably follows from considerations of attenuation properties in plate interiors.

c) testing by simulation

Simulations are a helpful tool. It could be commented, however, that simulating low-magnitude earthquake swarms for the rapakivi granite would not especially help PSHA there. The sparse data available for the surrounding crust, onshore and offshore, could possibly be fitted to a number of synthetic earthquake catalogs. On the other hand, to question the validity of the seismicity model, for example: Is the exponential function of earthquake magnitude justified here?

Comments on area source no. 10 after the videoconference on 15 January 2020

There was a recollection at STUK that the Wiborg rapakivi granite was not separated from the surrounding crust in the PSHA work carried out in the 1980s. The present consensus was that the special geology and seismicity features warrant a separate area source. Some related issues are as follows:

Does the lack of seismicity in the eastern part follow from a lack of earthquakes or a lack of earthquake reporting?

The boundaries displayed in Figure 1 would be justified if earthquake reporting was far more incomplete in the eastern than the western part. The Finnish-Russian border is located in the east, and has been defined according to various peace treaties throughout the centuries. Country borders complicate the assessment of seismicity at all times, and pre-instrumental offshore seismicity is difficult to parameterize. These aspects support the notion that seismicity may have been documented unevenly over the area. It can be noticed that one pre-instrumental swarm is located at some distance to the east of the area, though. No attempts to uncover hitherto unknown documentation in the eastern part have been carried out.

Possible migration of swarm activity

Even if the lack of earthquakes in the eastern part was a real feature during the time span of the available seismicity record, the spatial seismicity pattern could vary over time. It is demanding to argue convincingly either for or against spatial variability of earthquake swarms in the rapakivi granite area.

Level of observed seismicity

It was commented that the largest earthquake magnitudes of the swarms have been below magnitude M3. Strictly speaking this holds true for the instrumental era. During the Lapinjärvi swarm of 1951-52 in the pre-instrumental era, earthquakes with magnitudes above 3 most probably occurred. For example, knocked-down chimneys were reported. The most severe possible consequences of the swarms remain an open question.

Is there any relation between small and large earthquakes?

An interesting question for PSHA is whether the rapakivi structure, or the surrounding crust, could produce a moderate-to-large magnitude earthquake different from the shallow swarm-type activity.

The different open questions and uncertainties related to the seismic potential of area source no. 10 should be incorporated in the final logic-tree.

On the following day Simon reported on a related comment from Dr Varpasuo, in whose opinion "extrapolating G-R from the swarms should not be done up to high magnitudes. In fact, he originally ignored the swarms as not to skew the G-R parameters". It can be commented that the deviation of the swarms from the Poissonian model is well recognized. The narrow magnitude range and sparsity of available data constitute a problem, which in practice hinders calculation of the *b*-value.

Comment on seismic fault sources in Fennoscandia (for the future)

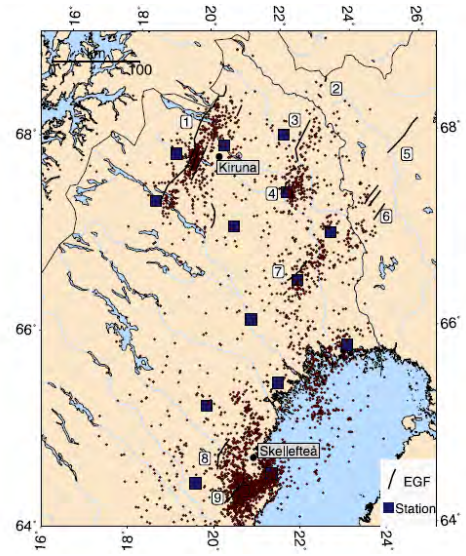

Figure 3. *Earthquakes registered in northern Sweden between 2000 and 2013 (brown dots). Blue squares denote permanent seismic stations of the Swedish National Seismic Network. Endglacial faults (EGF) are shown by black lines and are 1: Pärvie, 2: Palojärvi/Kultima, 3: Lainio-Suijavaara, 4: Merasjärvi, 5: Suasselkä, 6: Pasmajärvi, 7: Lansjärv, 8: Röjnöret, 9: Burträsk. From Lindblom et al. 2015*

Seismic area sources are the prevalent choice for PSHA in the Fennoscandian Shield. It may be noted, however, that the denser seismic networks of present time have led to improved accuracy of earthquake location: the fuzzy clouds of epicenters displayed on former seismicity maps sharpen up. It can sometimes be observed that the epicenters gather along endglacial faults (EGF; alternatively, 'post-glacial faults') in Sweden in particular. Currently the most active fault in Sweden is the Burträsk fault (no. 9 in Fig. 3). Lindblom et al. (2015) reported that there is a remarkable correlation between the present-day seismicity and the EGFs mapped in northern Sweden. They reported earthquake magnitudes below M_L3 in the proximity of the Pärvie fault (no. 1 in Fig. 3). Afonin et al. (2017) investigated the 48-km long Suasselkä fault (no. 5), which is the most prominent EGF in the Finnish

territory. Their network recorded some minor seismicity along the Suasselkä fault, and they concluded that the fault is seismically active. This kind of observations suggest that defining seismic fault zones may become an option in the future; however, it is not obvious whether the models of slip rates and characteristic earthquakes apply.

The maximum earthquake associated with the Pärvie fault has been estimated at magnitude 8 ± 0.4 (Lindblom et al. 2015). The maximum magnitudes related to the EGFs in Fennoscandia have been dated to ca. 9-11 ka before present and are associated with the deglaciation of the Weichselian ice sheet. They thus belonged to a different seismotectonic regime from the current one, and the standard practice is not to consider them in PSHA.

References

Afonin N, Kozlovskaya E, Kukkonen I, and DAFNE/FINLAND Working Group (2017) Structure of the Suasselkä postglacial fault in northern Finland obtained by analysis of local events and ambient seismic noise, *Solid Earth* **8**:531-544. doi: 10.5194/se-8-531-2017

Bommer JJ, Strasser FO, Pagani M, Monelli D (2013) Quality assurance for logic-tree implementation in probabilistic seismic-hazard analysis for nuclear applications: A practical example, *Seism. Res. Lett.* **84**:938-945. doi: 10.1785/0220130088

Elo S, Korja A (1993) Geophysical interpretation of the crustal and upper mantle structure in the Wiborg rapakivi granite area, southeastern Finland, *Precambrian Res.* **64**:273-288.

IAEA (International Atomic Energy Agency) (2010) Seismic hazards in site evaluation for nuclear installations, Specific Safety Guide No. SSG-9, IAEA, Vienna.

Korja A, Kosonen E (Eds) (2015) Seismotectonic framework and seismic source area models in Fennoscandia, northern Europe, Report S-63, Institute of Seismology, University of Helsinki.

Korja A, Kihlman S, Oinonen K (Eds) (2018) Seismic source areas for seismic hazard assessment in central Fennoscandia, Report S-66, Institute of Seismology, University of Helsinki.

Lindblom E, Lund B, Tryggvason A, Uski M, Bödvarsson R, Juhlin C, Roberts R (2015) Microearthquakes illuminate the deep structure of the endglacial Pärvie fault, northern Sweden, *Geophys. J. Int.* **201**:1704-1716. doi: 10.1093/gji/ggv112

Mäntyniemi P, Wahlström R (2013) Macroseismic reports and intensity assessments for the earthquakes in the Bay of Bothnia area, northern Europe on 15 and 23 June 1882, Report S-57, Institute of Seismology, University of Helsinki.

Musson RMW (2000) Evaluation of seismic hazard source models, In Lapajne JK and Vidrih R (Eds) Seismicity modelling in seismic hazard mapping, Slovenian Geophysical Survey, Ljubljana, 53-66.

Pagani M, Woessner J, Danciu L, Sørensen MB, Grünthal G, Arvidsson R (2010) Input specifications for seismic hazard computation, Deliverable D5.1, SHARE project, http://www.share-eu.org/sites/default/files/D5.1_SHARE.pdf

Appendix 3.3 Notes on Proposed Treatment of λ and β in Logic Tree

Gabriel R. Toro – May 5, 2019

This document provides more details on the proposed treatment of correlation between λ and β in the SENSEI logic trees.

Let λ and β be the best-estimates of the rate of earthquakes above the magnitude M_{min} used in the recurrence calculations and the Gutenberg-Richter slope in natural logarithmic space. These are the values tabulated in numerous reports. Let ρ be their correlation coefficient, which can be calculated from their covariance (which is provided in Appendix 2 of NE-4459 and Appendix 5 of S-64 [1]), and is calculated as follows:

$$\rho = \frac{COV(\beta, \lambda)}{\sigma_\beta \, \sigma_\lambda}$$

all quantities entering the equation above are provided in the two report Appendices mentioned above.

Level 2 of the logic tree discretizes β using the Keefer-Bodily three-point distribution and using the marginal standard deviation σ_β. The values of β are for the three branches are β_H, β, and β_L (where H and L stand for high and low, respectively).

Level 3 of the logic tree is slightly more complicated because the value of β for each branch is known (from Level 2), so one needs to use the conditional distribution of λ, which has mean $m_{\lambda|\beta_i} = \lambda + \rho(\frac{\sigma_\lambda}{\sigma_\beta})(\beta_i - \beta)$ and standard deviation $\sigma_{\lambda|\beta_i} = \sigma_\lambda\sqrt{1-\rho^2}$, where β_i is the conditioning value of β (from Level 2). This conditional distribution is also discretized using the Keefer-Bodily three-point distribution. The resulting logic tree is shown in Figure 1.

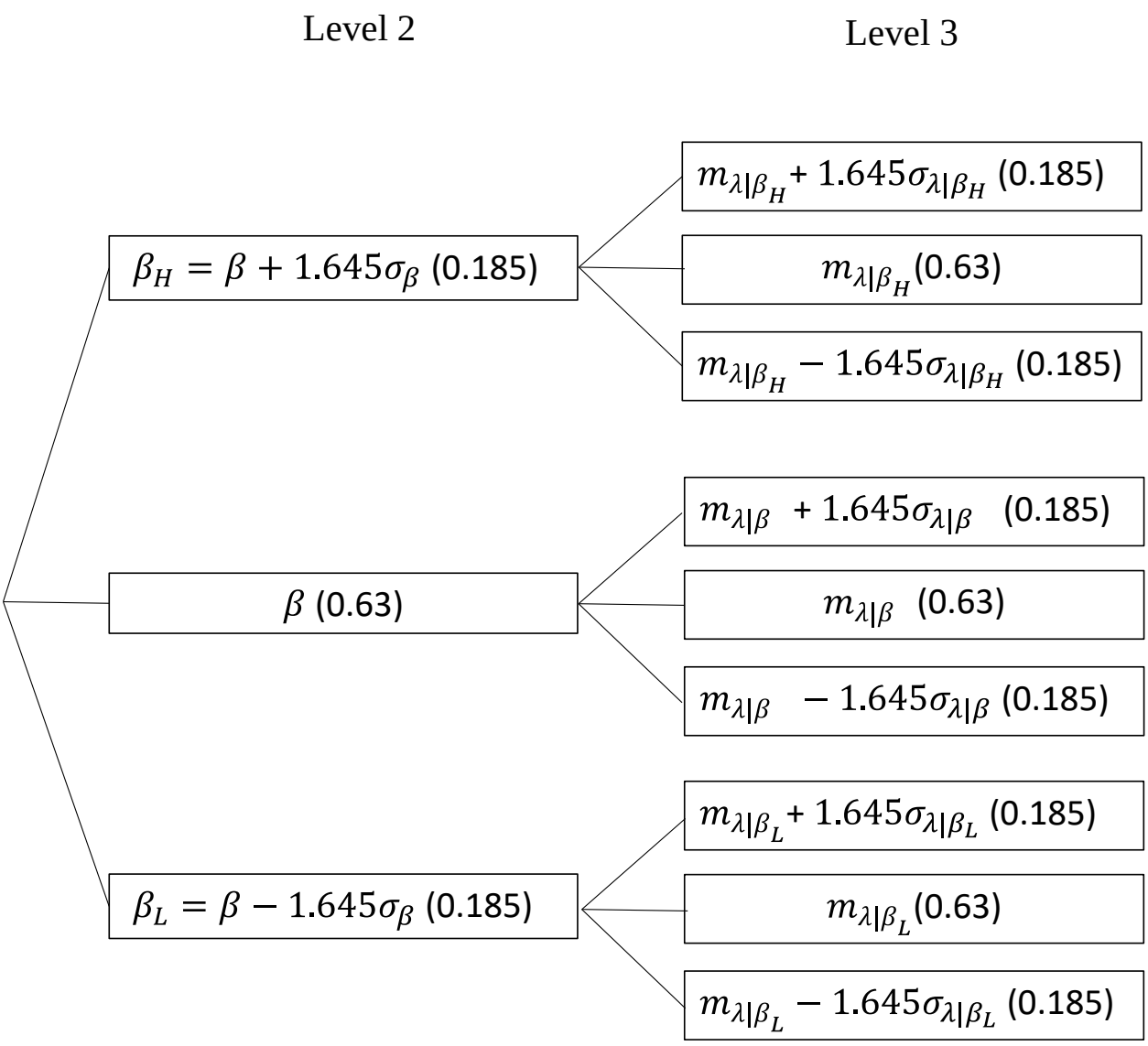

Figure 1. Logic tree for β and λ taking correlation into account.

The final step (if required by the software) is to convert the rate from $\lambda = \lambda\left[M > M_{\min_{recurrece}}\right]$ to $\lambda[M > M_{\min_{PSHA}}]$ (i.e., from the minimum magnitude used in the recurrence calculations to the minimum magnitude to use in the PSHA integration. This is done by applying the equation

$$\lambda\left[M > M_{\min_{PSHA}}\right] = \lambda\left[M > M_{\min_{recurrence}}\right] \exp\left\{-\beta(M_{\min_{PSHA}} - M_{\min_{recurrence}})\right\}$$

to each of the 9 β-λ pairs resulting from Levels 2 and 3 of the logic tree.

[1] Korja, A., Kihlman, S., Oinonen, K. (Eds) (2016). Seismic source areas in central Fennoscandia. Report S-64, Institute of Seismology, University of Helsinki, Helsinki, Finland (non-public).

Appendix 3.4

Appendix 3.4. On the depth distribution of earthquakes in Finland

P. Mäntyniemi, L. Fülöp, O. Kaisko, G. Toro 11 March 2020

Issue raised by expert group: **Line 29 in the SENSEI excel table**
"As discussed in the 2nd meeting, the focal depth / depth range of the site zone will probably have a significant impact on the results. The current calculations use a broad depth range."

Suggested resolution by expert group
"Sensitivity analyses using a mean focal depth of about 8 km (check earthquake data); for instance 6 < h < 10 .
Note added by Gabriel (May 29, 2019): figure 9.4.1 of Hanhikivi report S-61 shows a median depth of ~ 8 km, which supports the mean value suggested above (which corresponds to a uniform depth distribution between 0 and 16 km)."

Possible alternatives for the focal depth distributions

1. *A short history of focal depth determination in Fennoscandia*

An older notion on focal depths of earthquakes in the Fennoscandian Shield was that they are rather shallow. The uncertainties of depths determined using standard least-square location methods with sparse seismograph networks can be large, though, and many depths were fixed to 10 km. Macroseismic depth determinations could be attempted for the larger (M>4) pre-instrumental earthquakes that were widely observed and reported since the late 1800s. The depths were determined using the spacing of at least three isoseismals. These depths tend to be deeper, for example, a depth of 30 km was given to the central Finland earthquake of 1931 (Mäntyniemi 2004), but the corresponding uncertainties are typically large (± 10 km in this case).

The advent of synthetic seismogram modelling lead to more reliable depth estimates. Arvidsson et al. (1992) obtained focal depths in the lower crust for earthquakes in southern Sweden, and Arvidsson and Kulhanek (1994) gave a depth distribution between 11 and 37 km for seven earthquakes, some of which were located on the eastern coast of Sweden. Uski et al. (2012) estimated that earthquakes typically occur over the depth range of 14-30 km in Kuusamo in the Archean Karelian bedrock in NE Finland. The more reliable depth estimates question the validity of the old notion on focal depth distributions.

2. *NPP sites in Finland*

The vicinities of the three nuclear power plant (NPP) sites in Finland exhibit different seismicity features and depth ranges (Figs. 1, 2). Many earthquake swarms have been observed in the Wiborg rapakivi massif surrounding the Loviisa NPP in the south-east in the pre-instrumental and instrumental eras. They are very shallow, typically located in the uppermost few kilometres. Very little seismicity is recorded around Eurajoki in western Finland, and the few observations available are shallow. The northern site, Hanhikivi, in the municipality of Pyhäjoki is situated in a very different environment, where also deeper earthquakes have been recorded. The depth distribution extends down to almost 36 km according to available data. Deeper earthquakes have also been recorded on the eastern coast of Sweden and the Gulf of Bothnia.

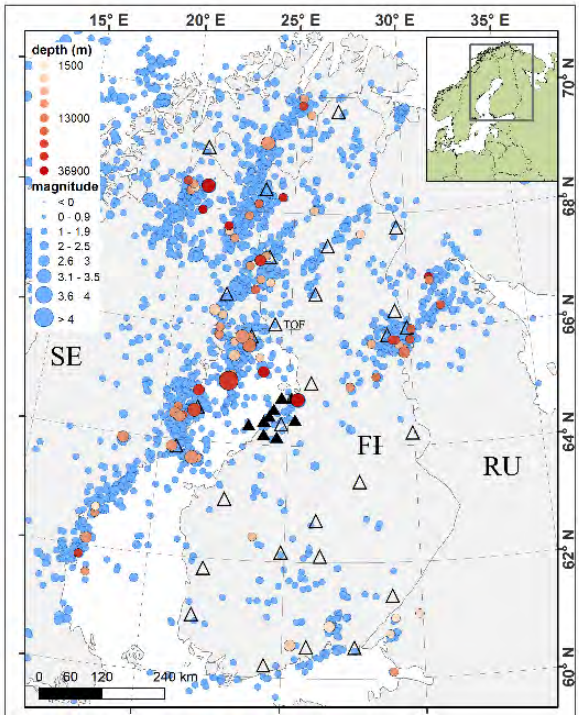

Figure 1a). *Epicenters of the Fennoscandian dataset between 2006 and 2018. Red dots show earthquakes with $M_L \geq 2$ accepted for the final analysis of Fenno-G16, and blue dots show smaller earthquakes. Triangles denote the seismic stations where data were obtained at 100-Hz or250-Hz sampling rate. The filled triangles compose the OBF network that operates around the planned NPP site in Pyhäjoki.*

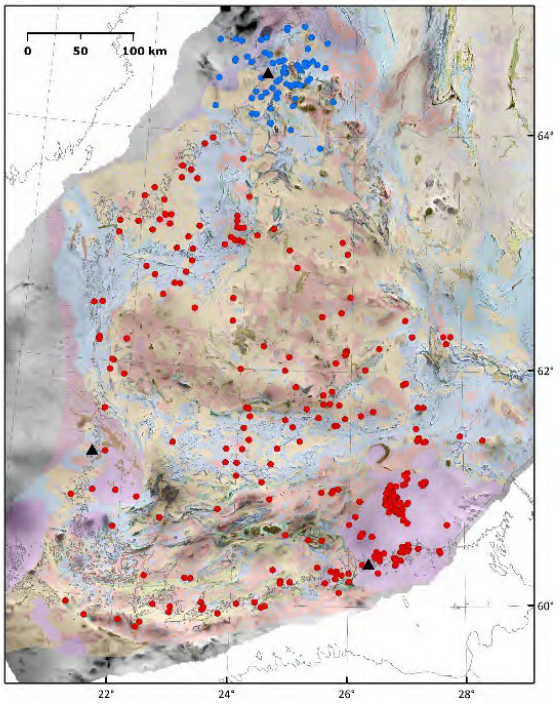

Figure 1b). *Black triangles show the three NPP sites in Finland. Blue dots show the reported earthquakes in the OBF annual reports (Valtonen et al. 2014; Vuorinen et al. 2015, 2016, 2018; Kaisko et al. 2017). Red dots show the earthquakes selected for the depth distribution in Southern Finland (Data: Ahjos and Uski 1992, ISUH 2018); only reliable depth determinations are used. Basemap: bedrock map of Finland (Nironen et al. 2016) shaded with the magnetic anomaly map (Airo 2005).*

Appendix 3.4

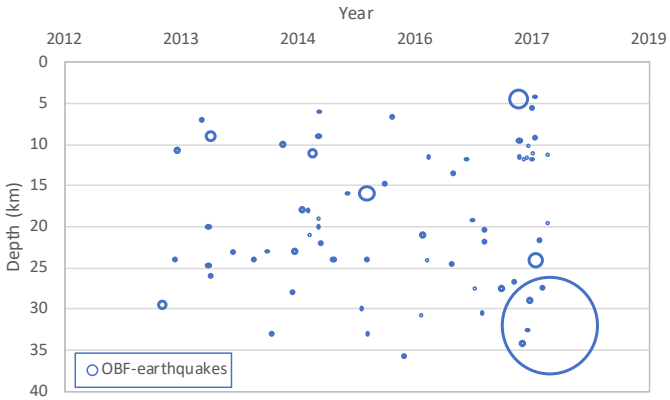

Figure 1c). *Depths of earthquakes in the vicinity of the NPP site in Pyhäjoki recorded by the OBF local seismic network (Blue dots from Figure 1B). There is an M_L 3.2 event (d=32km), seven events in the range M_L0.7-1.7 (d=4.5-34.2km), other events are M_L0.5 to M_L-0.7. Circle sizes are proportional to 10^M_L.*

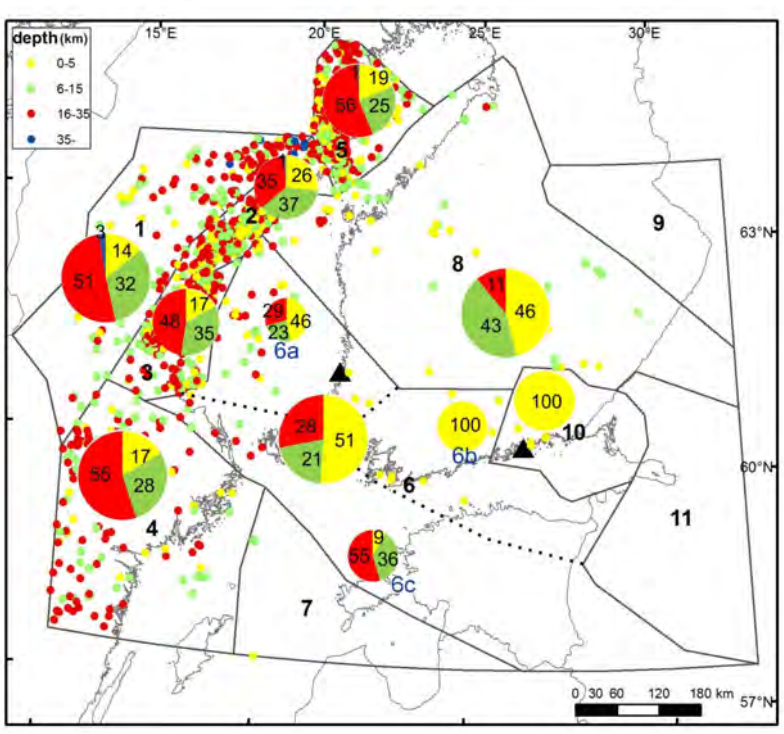

Figure 2. *Focal depth distribution of earthquakes in 2000-2012. Colour coding approximates the division between upper crust (yellow and green), middle crust (red), and lower crust (blue) sources. Pie charts show the proportion of events within each depth class. Depths routinely fixed to 10 km are not included. Reproduced Figure 6.4.1. from Korja et al. (2018).*

3. Depth distribution for Fennoscandian earthquakes (subset used for the Fenno-G16 GMPE)

The earthquake dataset used for the Fenno-G16 GMPE (from 2006 onwards) has been extended with events between M1.5 and M2, resulting in a total of 188 events. A bias has been noticed in the data for 5km and 10km in the meeting with the SENSEI Expert group (06.06.2019). There are two main reasons for the high frequencies at depths 2 km, 5 km, and 10 km. Firstly, the swarm-related events in the rapakivi massif are numerous and shallow. The ongoing seismic activity began in December 2011, and these events dominate the depth distribution of all earthquakes in the 2010s. It is questionable whether they should be included in the calculation of a mean/median depth for the other two NPP regions. Figure 3 shows the depths of earthquakes in seismic source area no. 10 discussed in the separate internal working document *On seismic source areas in the Fennoscandian Shield, with focus on the Loviisa NPP*. Pre-instrumental earthquakes seem to be deeper, but they have larger associated uncertainties. The available textual materials tell us that strong earthquake-related audible effects were observed also in these cases, which suggests that the events were shallow.

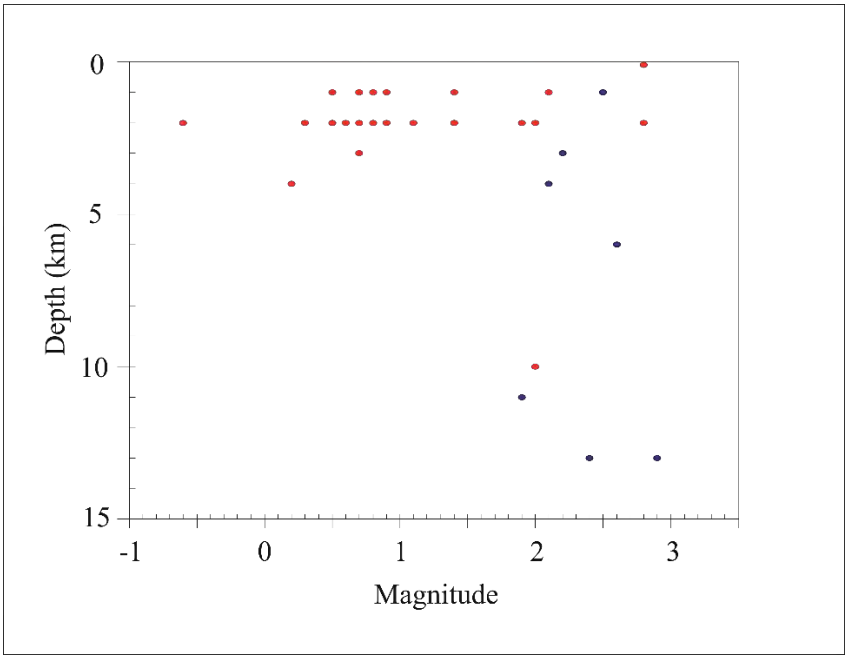

Figure 3. *Depths of earthquakes in the seismic source area no. 10 discussed in a separate internal SENSEI working document. Blue dots denote pre-instrumental and red dots instrumental earthquakes.*

Secondly, large azimuthal gaps in the earthquake epicentre vs. seismic station configuration deteriorate the quality of depth determination. This phenomenon is well recognized. Global seismic bulletins typically indicate depths fixed at 10 km or 33 km, whereas in Finnish bulletins the depth of 10 km is typically used. Because of the high frequencies at some depth values, we used two data sets, the first with all 188 earthquakes and the second without depths 2 km, 5 km, and 10 km.

Figure 4 shows the depth distributions for the entire dataset of 188 events, and for two subsets with events south of latitude 63ºN (42 events) and north of it (146 events). Latitude 63º runs about midway between Hanhikivi and Olkiluoto, about 200 km from both plants; Loviisa is situated further southward. Hence, depth distribution "North" is relevant for Hanhikivi and "South" for Olkiluoto and Loviisa. One M_w1.8 event in the South subset has an assigned depth of 0km, which is problematic for the log transformation. This depth was manually re-assigned to 0.5km, which is within the depth determination error and should preserve the influence of a very shallow earthquake in the dataset.

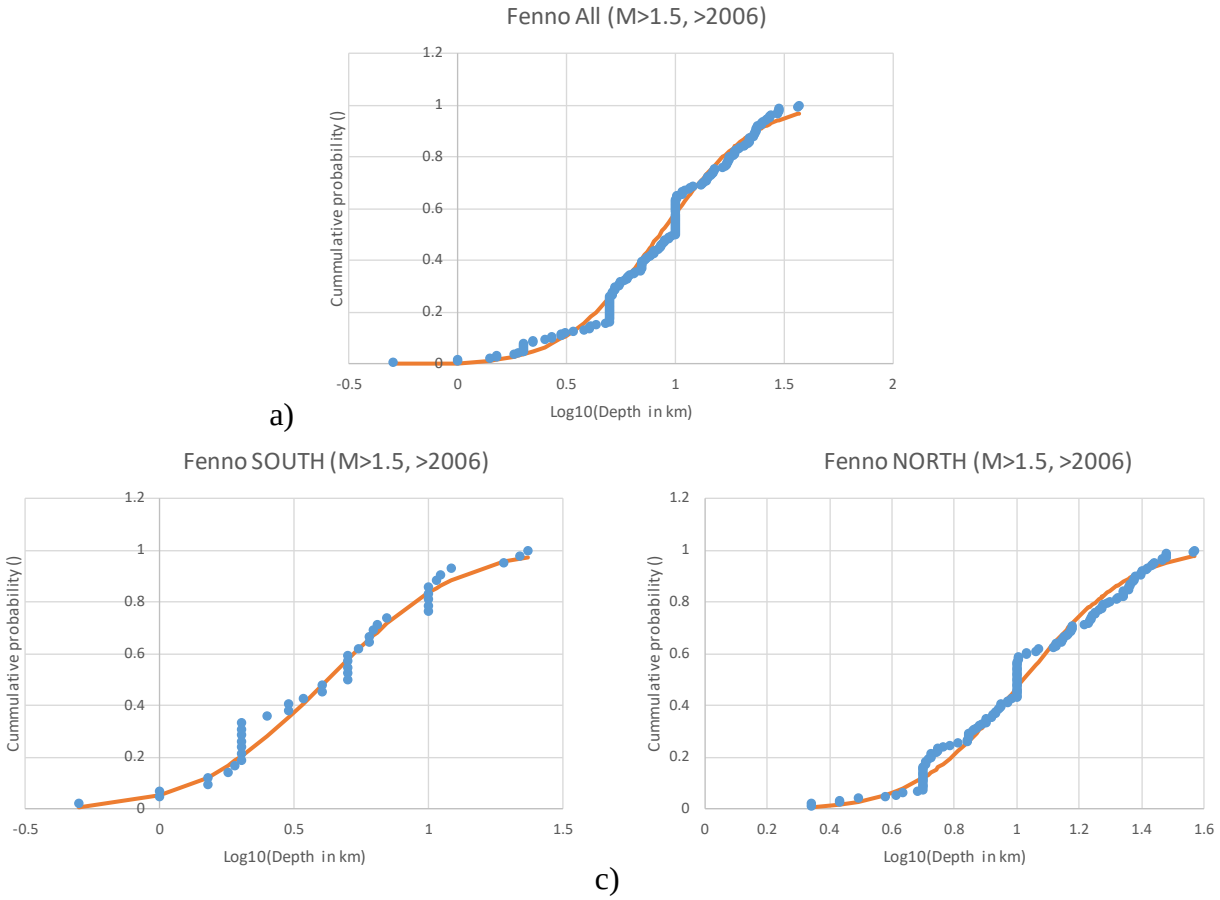

Figure 4. *Normal distribution fitted to Log10(Depth), CDF(orange) to the Fennoscandian data.*

It can be noticed that the North dataset dominates the data. The magnitude distribution is similar with mean M_w ~ 2 (Table 1); the depths correspond to a similar earthquake size in the North and South

sub-regions. The overall median of the depth is 10km, and 10km for the North and 5km for the South set. The mean depths are $\log_{10}(d_{North})=1.0205$ (in km) and $\log_{10}(d_{South})=0.6227$ (Table 1).

Table 1. Earthquakes with magnitude M_w >1.5 in Fennoscandia since 2006 (same data as in Figure 4).

Data	Mean M_w	STD M_w	Median $\log_{10}$(d)	Mean $\log_{10}$(d)	STD $\log_{10}$(d)
All 188 events	2.01	0.5019	1.0 (d=10km)	0.9336	0.3375
NORTH (>63°) 146 events	2.01	0.5046	1.0 (d=10km)	1.0205	0.2746
SOUTH (>63°) 42 events	2.01	0.4981	0.6990 (d=5km)	0.6227	0.3848

Figure 5 shows the corresponding depth distributions for the second dataset. The mean and standard deviation in Table 2 are not significantly different from those of the complete dataset. Means are about the same and standard deviations slightly increased, as expected. In addition, Figure 5d gives the depth distribution of 24 events within 200 km from Hanhikivi.

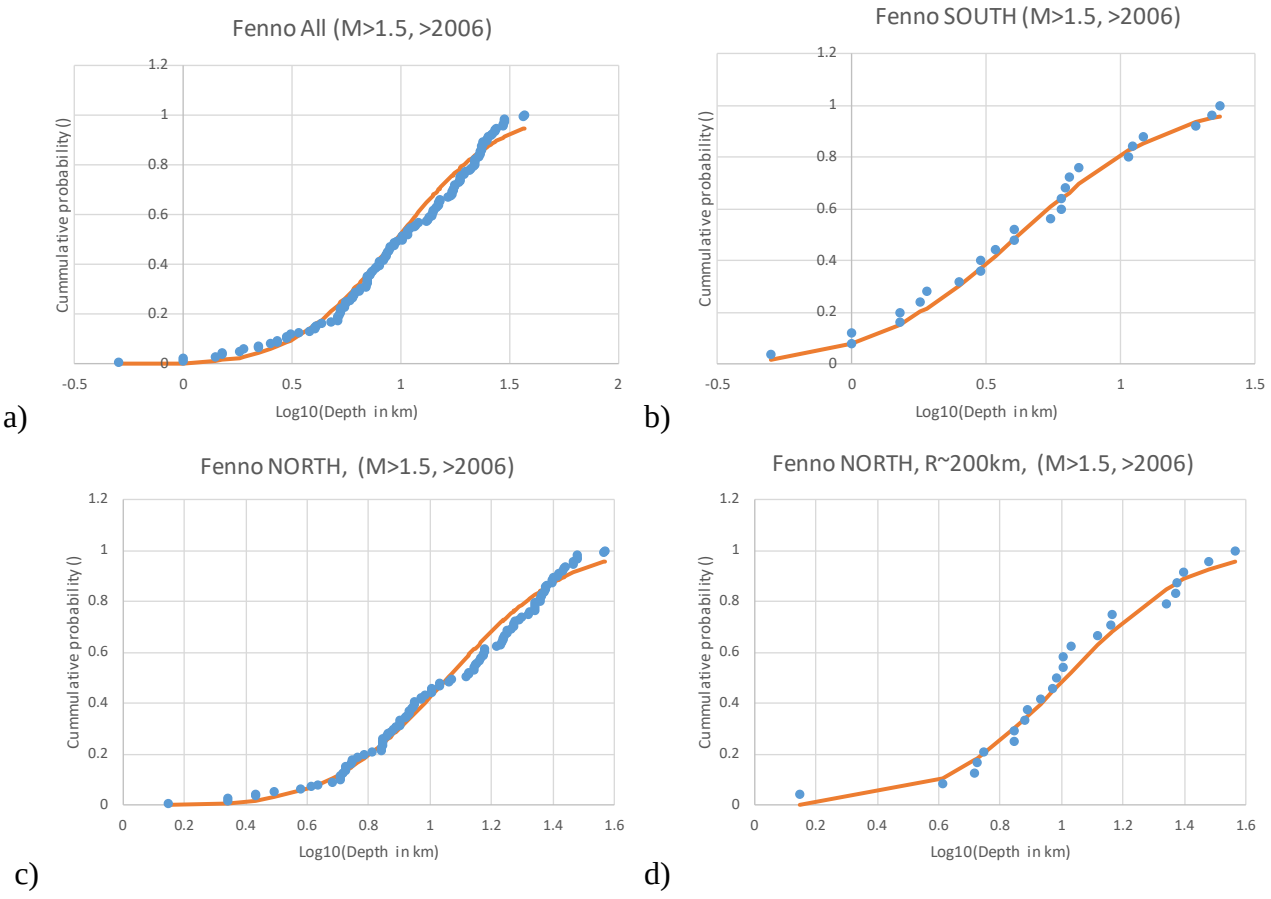

Figure 5. *Normal distribution fitted to Log10(Depth), CDF(orange) for the second Fennoscandian dataset. In addition Figure 5d gives the depth distribution of 24 events within 200km of Hanhikivi.*

Appendix 3.4

Table 2. Earthquakes with magnitude M_w >1.5 in Fennoscandia since 2006 (same data as in Figure 5).

Data	Mean M_{cat}	STD M_{cat}	Median $\log_{10}$(d)	Mean $\log_{10}$(d)	STD $\log_{10}$(d)
All 136 events	1.99	0.4939	-	0.9771	0.3700
NORTH (>63°) 111 events	1.97	0.4801	-	1.0653	0.2902
NORTH (<200km) 24 events	2.23	0.7202	-	1.0122	0.3193
SOUTH (>63°) 25 events	2.04	0.5583	-	0.6221	0.4381

4. *Depth distribution for earthquakes in the NGA-East dataset on Vs~2000m/s, used for Fenno-G16 GMPE*

This section is added to confirm that the combined Finnish and NGA-East data used for the Fenno-G16 GMPE do not have very different depth distributions. This is not an argument for any choice of depth distribution in Finland. The NGA-East events used together with Fennoscandian data in the calibration of FennoG-16 are given in Table 3. Several events have no specified depth in the NGA-database (Goulet at al. 2014).

Table 3. All earthquakes with a closest station Vs30~2000m/s in the NGA-East dataset (Goulet at al, 2014)

Date & Earthquake	M_w	Depth(km)*	V_{s30} of closest station (m/s)
Cobourg_2007-07-19	2.8	5	2000
LaMalbaie_1997-10-28	4.29	5	2000
Nahanni_1985-12-23a	5.1	6	1700
LaMalbaie_1997-08-20	3.27	7.5	2000
Charlevoix_2001-05-22	3.6	11.4	2000
LaMalbaie_2000-06-15	3.29	11.4	2000
RiviereDuLoup_2005-03-06	4.65	13.3	2000
BaieStPaul_2002-08-17	3.24	13.3	2000
BaieStPaul_2008-01-03	2.77	13.5	2000
ValDesBois_2010-06-24	2.57	16.7	2000
BarkLake_2003-10-12	3.82	18	2000
Buckingham_2008-06-11	2.97	18	2000
Hawkesbury_2006-02-26	2.59	18	2000
Laurentide_2000-07-12	3.65	18	2000
Laurentide_2000-07-12A	3.11	18	2000
StFlavien_2010-07-23	3.51	19.5	2000
ValDesBois_2010-07-22	2.37	19.9	2000
LaBaie_2004-05-04	2.87	22	2000
ConstanceBay_2009-05-08	2.57	26.1	2000
Saguenay_1988-11-23	4.19	28	2000
Saguenay_1988-11-25	5.85	29	2000

Appendix 3.4

Saguenay_1988-11-26	3.53	30	2000
BaieStPaul_2006-04-07	3.72	25	2000
CapRouge_1997-11-06	4.45	21.7	2000
EagleLake_2006-07-14	3.46	17	2000
Hawkesbury_2011-03-16	3.59	7.5	2000
LaMalbaie_2003-06-13	3.53	10.2	2000
Nahanni_1985-12-23	6.76	8	1700
Nahanni_1985-12-25	5.15	7	1700
PortHope_2004-08-04	3.12	4	2000
RiviereDuLoup_2008-11-15	3.57	14	2000
Thurso_2006-02-25	3.7	20	2000
ValDesBois_2010-06-23	5.1	18.7	1700

- Depth is the hypocenter depth reported in the NGE-East Flat-file, or re-calculated from the epicenter and hypocenter distance given in the Flat-file

Figure 6 shows the depth distributions of these NGA-East events and Fennoscandian events of comparative magnitude (M_w>2.37). In Figure 6a all Fennoscandian events were included, while for Figure 6b the Fennoscandian events with depths 2km, 5km and 10km were removed. The comparisons reveal a larger spread of the depths in Fennoscandia, but a comparable mean.

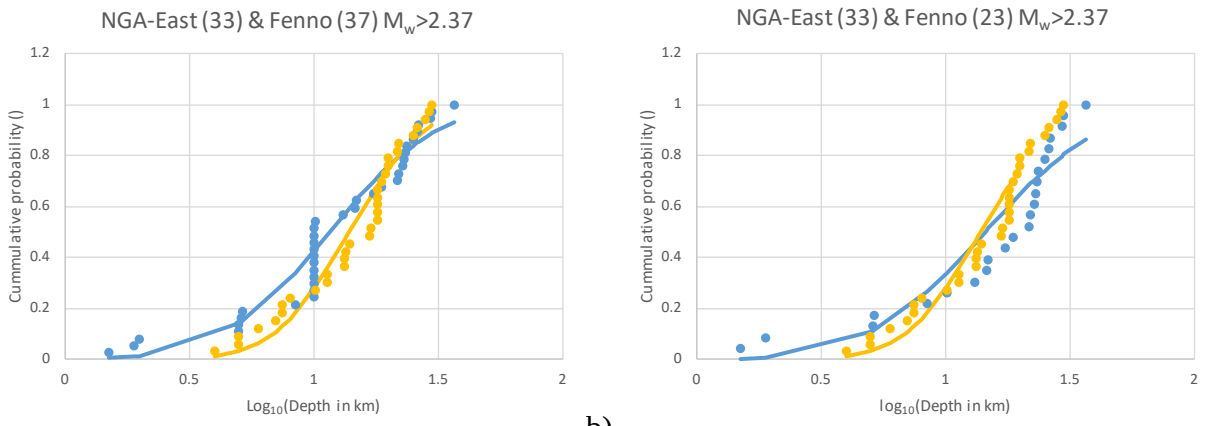

a) b)

Figure 6. *Normal distribution fitted to Log10(Depth). Blue dots are the Finnish data and blue lines the CDF fit to it. Yellow are the NGA-East points and the corresponding CDF fit. In (a) for the Finnish data Median=1, Mean=1.063595589 and STD=0.338648527; in (b) for the Finnish data Median=1, Mean=1.158872469 and STD= 0.37098742. For the NGA-East data Mean=1.142256491 and STD=0.239234357 in both figures.*

5. *Additional geophysical arguments*

Appendix 3.4

Lamontagne and Ranalli (1996) defined the seismogenic zone as the depth range over which 99% of earthquakes occur. Following this definition, Korja (2015) gave the thickness of the seismogenic zone as 31 km in the region with a 500-km radius surrounding the Hanhikivi site. The depth data used covered the years 2000-2012. This concept is not sensitive to the uncertainty of depth estimation; for example, Kaikkonen et al. (2000) used local earthquake data from 1965-1997 and gave an equal value of 31 km, although the spacing of seismic stations was far less dense in the past and, consequently, the uncertainties of earthquake parameters were larger.

Earthquake depths may give clues as to the thermal conditions of the lithosphere; alternatively, the depth below which the ductile transformation dominates over brittle transformation is often considered a temperature isotherm. Veikkolainen et al. (2017) investigated the seismicity cut-off depth and heat flow in Fennoscandia. They used five data sets of seismicity data from the years 2000-2015 (Fig. 7a). (The selected areas do not include the NPP sites in southern Finland.) The earthquake epicentres were assigned surface heat flow values from an interpolated heat flow grid. The average cut-off depth from all five areas was given as 28±4 km, with some variation between the investigated areas (Fig. 7b). It is suggested that this value can be used to approximate the depth of the temperature isotherm of 350 °C in the Fennoscandian conditions. The highest occurrence of earthquakes is obtained in regions with the corrected heat flow over the range of 48-60 mWm^{-2}. In general, there does not seem to be any obvious correlation between heat flow and seismic cut-off depth. Also deep earthquakes (depth > 25 km) occur in areas of different heat flow.

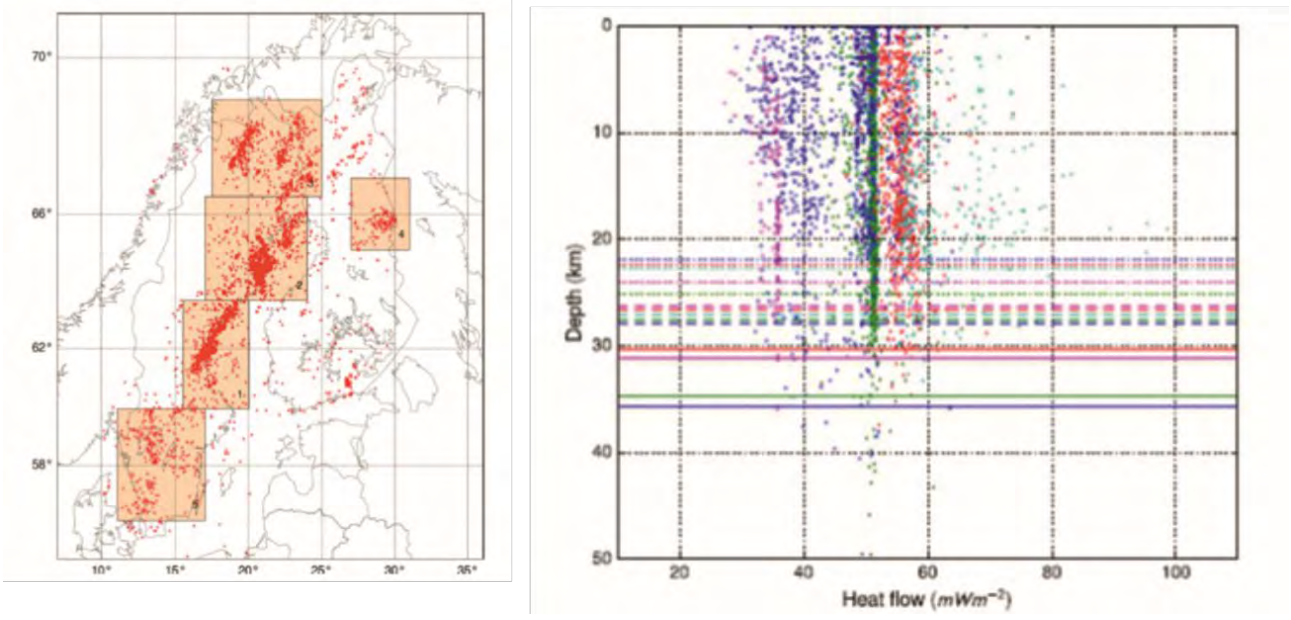

a) b)

Figure 7. *a) The rectangles '1','2','3','4' and '5' (corresponding to southern Gulf of Bothnia, northern Gulf of Bothnia, Lapland, Kuusamo area and southern Sweden, respectively) show where heat flow and seismicity data were investigated by Veikkolainen et al. (2017). b) Palaeoclimatically corrected heat flow in comparison with the earthquake depths in the five study areas. Area 1 is red, 2 green, 3 blue, 4 pink and 5 cyan. Dotted lines, dashed lines and solid lines indicate the 90th, 95th and 99th percentiles of focal depths for all five data sets. Both figures are from Veikkolainen et al. (2017).*

The depth distributions of the five areas show variation in the mean depth from 10.6 km in northern Sweden to 15.3 km in Kuusamo (Fig. 7). This suggests that using depth averages over very large areas may not be a very good approach, even though the comparison of the data in Figure 5c and Figure 5d does not suggest significant differences between the general data for the North of Finland and the region 200km around Hanhikivi NPP. All the distributions in Figure 8 peak at the depths of 15-25 km, corresponding to the depths where the earthquake mechanism transforms from slick slip to stable sliding, at temperatures of 200-300 °C.

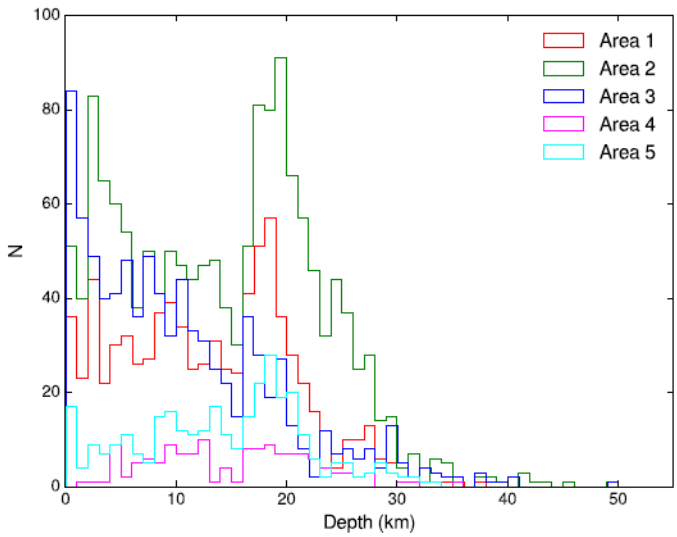

Figure 8. *The earthquake depth distributions of earthquakes in the five areas. From Veikkolainen et al. (2017)*

6. Suggested depth distribution scheme for the SENSEI sensitivity calculation

Based on the above data and comparisons, we suggest distinguishing the depth distributions North and South for the PSHA calculations (Table 4, values copied from Table 2); however, there are no sufficient data to estimate separate depth distributions for Olkiluoto and Loviisa.

For Hanhikivi (North) events located in the vicinity of the site (<200km) can be used (Table 4, values copied from Table 2). The distribution of these events does not differ significantly from the depth

distribution for the general North region (Table 2). This observation is contradicted by the investigation of Veikkolainen et al. (2017), which shows differences between the specific areas in the North. Their smaller specific areas and the coarse division of the Finnish territory used here may explain some of the difference.

Table 4. Suggested depth profile for the SENSEI sensitivity models for the North (Hanhikivi) and South of Finland (Olkiluoto and Loviisa)

	Distribution parameters from the data		Depth range of uniform probability for SENSEI PSHA models between Mean ± 1·STD (*68% in this bounds*)	
	Mean $\log_{10}(d)$	STD $\log_{10}(d)$	d_{min}(km)	d_{max}(km)
SENSEI - North	1.0122	0.3193	5	21
SENSEI - South	0.6221	0.4381	1	11

EZ-FRISK defines the depth range using a minimum and maximum value. Between them, the uniform probability distribution is assumed. G. Toro derived uniform distributions that is equivalent in terms of hazard to the lognormal distributions with parameters given in Table 1 (presented as slides in the SENSEI meeting). Based on that study the single depth range of uniform probability distribution is proposed for the EZ-FRISK modes (Figure 9 and Table 5).

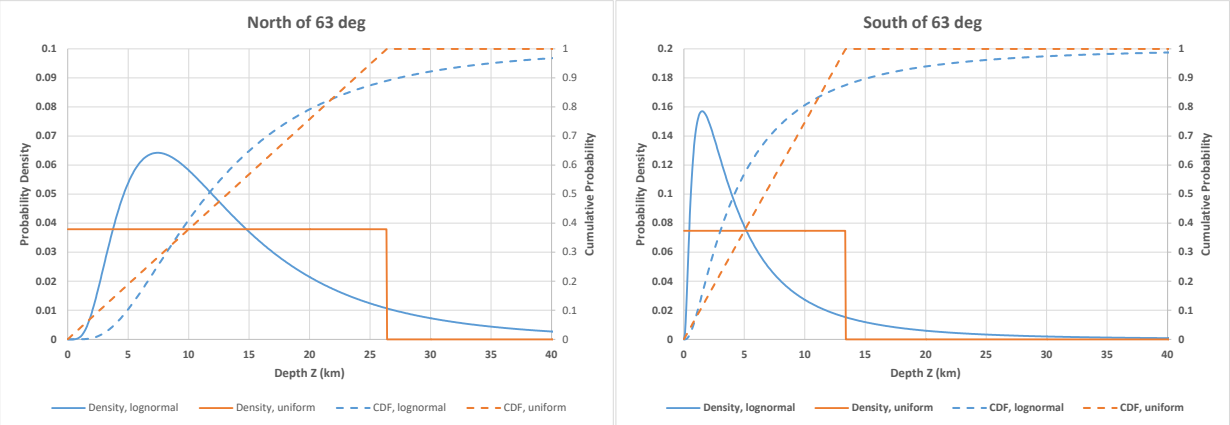

Figure 9. *Comparison of the uniform and lognormal distribution (G. Toro, SENSEI meeting slide)*

Table 5. EZ-FRISK input, for a single seismogenic layer of uniform probability distribution with depth, to SENSEI models for North (Hanhikivi) and South of Finland (Olkiluoto and Loviisa)

	Depth range of uniform probability for models in EZ-FRISK	
	d_{min}(km)	d_{max}(km)
SENSEI – North (Hanhikivi)	0	26
SENSEI – South (Olkiluoto and Loviisa)	0	13

Appendix 3.4

OpenQuake accepts discretized distribution of hypocentral depths. Each depth is associated with a probability of earthquake occurrence, so that the sum of all probabilities add up to unity. In OpenQuake, the lognormal distribution (or any distribution) can be modelled using discrete depths without adding significantly to the complexity of the input files. Of course, increasing the number of depths increases the computational cost (i.e. some sensitivity runs were done with 1, 5, 10 and 35 layers for the 35km depth in the Loviisa models). Based on that, it is suggested that the 35km depth be divided in 14 and the 45km depth in 18 layers with the probabilities shown in Table 6.

Table 6. OpenQuake input, for 14 seismogenic depths with the associated probabilities, to SENSEI models for North (Hanhikivi) and South of Finland (Olkiluoto and Loviisa)

	Probabilities for models in OpenQuake	
Depth (km)	SENSEI – North (Hanhikivi)	SENSEI – South (Olkiluoto and Loviisa)
1.25	1.49662E-02	1.53630E-01
3.75	8.30237E-02	2.86227E-01
6.25	1.54661E-01	2.08240E-01
8.75	1.62088E-01	1.19464E-01
11.25	1.36771E-01	7.26806E-02
13.75	1.07040E-01	4.69615E-02
16.25	8.16290E-02	3.19003E-02
18.75	6.18795E-02	2.25902E-02
21.25	4.70488E-02	1.65745E-02
23.75	3.60355E-02	1.25431E-02
26.25	2.78644E-02	9.75791E-03
28.75	2.17778E-02	7.78349E-03
31.25	1.72152E-02	6.35252E-03
33.75	1.37696E-02	5.29534E-03
36.25	1.11470E-02	
38.75	9.13515E-03	
41.25	7.57986E-03	
43.75	6.36851E-03	
	sum=1	sum=1

The data above correspond to the following tracing of the intended lognormal distribution:

Appendix 3.4

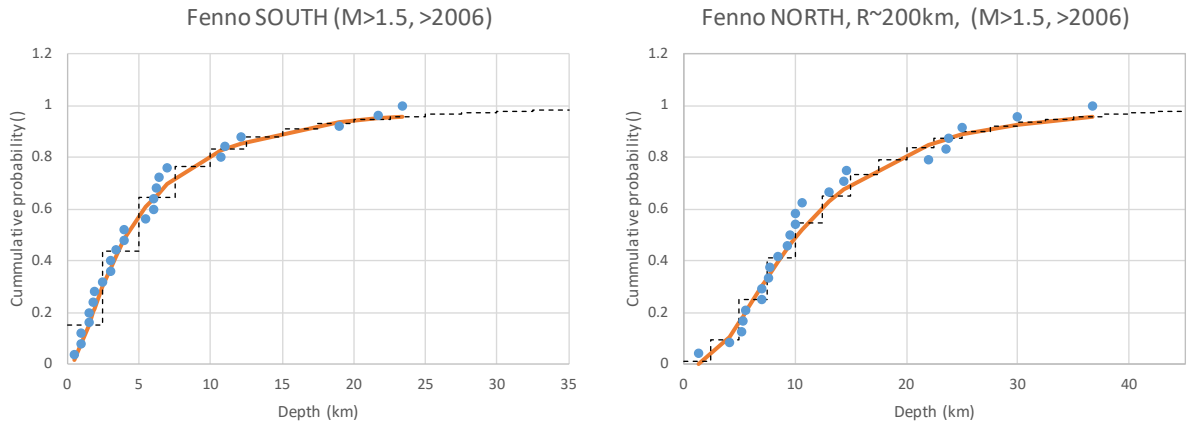

Figure 10. *Comparison of the lognormal distribution, plotted with parameters from Table 4, and the cumulative probabilities calculated from the OpenQuake input in Table5*

A computationally more efficient alternative would be to use the 9- or 10-point Miller-Rice distribution. The inputs for the 9-point Miller-Rice distribution is given in Table 7.

Table 7. OpenQuake input, for Miller–Rice discretization of the lognormal depths distribution truncated to 35km and 45km for South and North respectively. Depths and associated probabilities, to SENSEI models for North (Hanhikivi) and South of Finland (Olkiluoto and Loviisa)

SENSEI – North (Hanhikivi)		SENSEI – South (Olkiluoto and Loviisa)	
Depth (km)	Probabilities for OpenQuake	Depth (km)	Probabilities for OpenQuake
1.94783	0.034479	0.427927803	0.034479
3.494552	0.08599	0.954850028	0.08599
5.217781	0.130813	1.656266218	0.130813
7.333874	0.162023	2.645042734	0.162023
10.07523	0.173391	4.095902713	0.173391
13.78638	0.162023	6.315024481	0.162023
19.07774	0.130813	9.913379197	0.130813
27.14987	0.08599	16.29496392	0.08599
39.28756	0.034479	28.12157177	0.034479
	sum=1		sum=1

References

Ahjos T, Uski M (1992) Earthquakes in northern Europe in 1375-1989. Tectonophysics 207:1-23

Airo M-L (ed) (2005) Aerogeophysics in Finland 1972–2004: Methods, System Characteristics and Applications. Geological Survey of Finland, Special Paper 39:21-74

Arvidsson R, Wahlström R, Kulhanek O (1992) Deep-crustal earthquakes in the southern Baltic Shield. Geophys J Int 108(3):767-777

Arvidsson R, Kulhanek O (1994) Seismodynamics of Sweden deduced from earthquake focal mechanisms. Geophys J Int 116(2):377-392

Goulet CA, Kishida T, Ancheta TD, Cramer CH, Darragh RB, Silva WJ, Hashash YMA, Harmon J, Stewart JP, Wooddell KE, Youngs RR (2014) PEER NGA-East Database (No. PEER 2014/17). Pacific Earthquake Engineering Research Center, California, Berkeley.

ISUH (2018) Institute of Seismology, University of Helsinki, earthquake database.

Appendix 3.4

Kaikkonen P, Moisio K, Heeremans M (2000) Thermomechanical lithospheric structure of the central Fennoscandian Shield. Phys Earth Planet in 119:209-235

Kaisko O, Vuorinen T, Kortström J, Uski M, Tiira T (2017) OBF-verkon toiminta ja seismiset havainnot vuonna 2016, (The operation and seismic observations of the OBF-network in 2016). Report T-96, Institute of Seismology, University of Helsinki, Helsinki. (in Finnish)

Korja A (2015) Seismogenic zone, in Korja A, Kosonen E (Eds) Seismotectonic framework and seismic source area models in Fennoscandia, northern Europe, Report S-63, Institute of Seismology, University of Helsinki, pp.223-225.

Korja A, Kosonen E (Eds) (2015) Seismotectonic framework and seismic source area models in Fennoscandia, northern Europe. Report S-63, Institute of Seismology, University of Helsinki.

Korja A, Kihlman S, Oinonen K (Eds) (2016) Seismic source areas in central Fennoscandia. Report S-64, Institute of Seismology, University of Helsinki, Helsinki, Finland.

Lamontagne M, Ranalli G (1996) Thermal and rheological constraints on the earthquake depth distribution in the Charlevoix, Canada, intraplate seismic zone. Tectonophysics 257: 55-69

Mäntyniemi P (2004) Pre-instrumental earthquakes in a low-seismicity region: A reinvestigation of the macroseismic data for the 16 November 1931 events in Central Finland using statistical analysis. J Seismol 8:71-90

Nironen M, Kousa J, Luukas J, Lahtinen R (2016) Geological map of Finland – Bedrock, Geological Survey of Finland, Espoo.

Uski M, Tiira T, Grad M, Yliniemi J (2012) Crustal seismic structure and depth distribution of earthquakes in the Archean Kuusamo region, Fennoscandian Shield. J Geodyn 53:61-80

Valtonen O, Uski M, Kortström J, Korja A (2014) OBF-verkon toiminta ja seismiset havainnot vuonna 2013, (The operation and seismic observations of the OBF-network in 2013). Seismologian instituutti, raportti T-92. Helsinki, 29 pp. (in Finnish)

Veikkolainen T, Kukkonen IT, Tiira T (2017) Heat flow, seismic cut-off depth and thermal modeling of the Fennoscandian Shield. Geophys J Int 211:1414-1427. doi: 10.1093/gji/ggx373

Vuorinen T, Kaisko O, Uski M, Kortström J, Korja A (2015) OBF-verkon toiminta ja seismiset havainnot vuonna 2014 (The operation and seismic observations of the OBF-network in 2014). Report T- 94, Institute of Seismology, University of Helsinki, Helsinki. (in Finnish)

Vuorinen T, Uski M, Kortström J, Korja A (2016) OBF-verkon toiminta ja seismiset havainnot vuonna 2015, (The operation and seismic observations of the OBF-network in 2015). Report T-95, Institute of Seismology, University of Helsinki, Helsinki (in Finnish)

Vuorinen T, Kaisko O, Kortström J, Uski M, Tiira T (2018) OBF-verkon toiminta ja seismiset havainnot vuonna 2017, (The operation and seismic observations of the OBF-network in 2017). Report T-98, Institute of Seismology, University of Helsinki, Helsinki (in Finnish)

Appendix 3.5

Appendix 3.5 M_{max} using the Bayesian approach

L. Fülöp, (*in review with P. Mäntyniemi*)
18 May 2020

Issue raised by expert group:

The purpose of this document is to update the M_{max} estimates in the SENSEI project. The starting point of the calculations are the values presented by G. Toro in the Expert Group meeting (26. March 2020).

The main update to those estimates is the reformulation of the likelihood function based on the completeness time interval (T_i) of the seismicity record for each seismic source area (SSA). These completeness values are collected in the work document of the SENSEI project "On the completeness intervals of pre-instrumental seismicity records in Fennoscandia" P. Mäntyniemi, L. Fülöp 15 May 2020.

Using the new T_i's the composite likelihood function is calculated and compared to the earlier versions. In addition, the M_{max} distribution is re-evaluated and critically discussed in the conclusions.

- *Input parameters for the M_{max} estimation in the SENSEI project*

As presented by G. Toro in the 26th of March 2020 Expert Group meeting, the preliminary estimations of M_{max} in SENSEI were based on the notion that a separate M_{max} calculations are done for the Loviisa plus Olkiluoto SSA's (generically called "South") and for the Hanhikivi SSA's generically called "North".

In the Loviisa & Olkiluoto hazard study a single zoning was used, with SSA's numbered 1 to 11 (Korja and Kosonen, 2015). The Hanhikivi hazard study was based on two alternative zoning options called Model 1 and Model 2 (Korja *et al*, 2016). In addition to these original zonings, a merged zoning was created in the SENSEI project, by combing the Loviisa & Olkiluoto zoning map with Model 2 for Hanhikivi. This merged zoning cover the entire territory of Finland.

The input parameters for the M_{max} calculation of these three zoning options ("South", "North" and "Merged") are given below from the slides of G. Toro (26th March 2020). These input parameters were preliminary used for applying the Bayesian approach and the KSB approach to estimate the M_{max} for the "South", "North" and "Merged" regions respectively.

Table 1. Preliminary estimates of input parameters for the M_{max} calculation (G.Toro, 26th March 2020)

Appendix 3.5

Site	South (v.1)	South (v.2)	North (v.1)	North (v.2)	North (v.3)	Merged
M_{min}	0.9	0	1.1	0	0	0
$\lambda(M>M_{min})$	80.286	576.203988	84.457	2019.285556	1493.837251	1626.867201
β	2.960	2.471	2.533	2.399	2.415	2.447
T (yrs)	517.98	517.98	131	131	131	131
n (=λT)	41586.5	298462.1	11063.9	264526.4	195692.7	213119.6
Mmax,obs	4.5	4.5	4.3	4.3	4.3	4.5
α_0	0.625	0.988	0.965	1.000	0.998	0.970
Reference	Korja et al. (2016). Report S-64 (results for whole study region)	Calculation Group's combination of rates for S1-S11	Saari et al., (2015), NE-4459, Section 5.2.3 (whole study region for Hanhikivi)	Calculation Group's combination of rates for Hanhikivi Model 1	Calculation Group's combination of rates for Hanhikivi Model 2	Calculation Group's combination of rates for Hanhikivi Model 2 and South
Notes	Is T=517.98 justified? (see next slide)	Rate is not too different from v.1, but β is very different	Alternative Mmax,obs=5.9; P. Mäntyniemi, also provided slightly different estimates	Alternative Mmax,obs=5.9	Alternative Mmax,obs=5.9	Alternative Mmax,obs=5.9

- *Problem of the preliminary methodology and proposed solution*

The main inconsistency of the above procedure is that the completeness (T) is not unique for the SSA's. In practice each SSA "*i*" in these regions "South", North" and "Merged" has its own completeness interval (T_i). Especially for the SSA's in region "South", the differences between the completeness intervals are very large. Hence, a single input parameter as used above (e.g. above T=517.98 years and T=131 years) does not reflect the information known about the SSA's.

This issue of different completeness intervals is especially influencing the M_{max} likelihood function in the Bayesian approach. The solution proposed by G. Toro was to calculate the combined likelihood function as:

$$L(M_{max}) = \prod_i \left[1 - e^{-\beta_i (M_{max} - m_{0,i})}\right]^{-(\lambda_i T_i)} \qquad \text{(Eq. 1)}$$

Where:

- $\lambda_i, \beta_i, m_{0,i}$ are all tabulated and shown in recurrence appendices of the original hazard studies;
- T_i (sum of non-overlapping historical and instrumental intervals in zone *i*) not stated clearly, but can be obtained from recurrence appendices (+ knowledge of historical seismicity and its completeness)

- *Results*

The values of T_i and M_{maxi} for each SSA in the regions "South" and Model 2 "North", was collected in the work document of the SENSEI project "*On the completeness intervals of pre-instrumental seismicity records in Fennoscandia*" P. Mäntyniemi, L. Fülöp 15 May 2020. They are reproduced here:

Table 2. Estimates of completeness interval T_i for seismic source areas (SSA) in Fennoscandia.

"South"	M_{max}^{obs}	Year of M_{max}^{obs}	T_i	"North"-Model 2	M_{max}^{obs}	Year of M_{max}^{obs}	T_i
1	3.9	2014	183.1	2.1	3.3	1835	60.3
2	3.9	1751	189.2	2.2	4.0	1993	115.7
3	3.6	1886	202.6	2.3	3.5	1886	109.1
4	4.5	1497	242.6	2.4	3.7	1751	186.3
5	4.1	1909	177.9	2.5	4.0	1909	157.6
6	4.5	1976	185.4	2.6	4.2	1882	180.5
8	4.0	1931	181.9	2.7	4.1	1898	154.6
10	2.9	1952	50.5	2.8	3.7	1960	105.6
				2.9	4.3	1960	215.2
				2.10	3.6	1991	74.9
				2.11	3.9	1857	230.8
				2.12	2.9	1952	66.3

Base on this data, the likelihood function of each SSA was calculated and summarized according to Equation 1. The individual likelihood functions of each SSA is shown for the regions "South", "North Model 2" and the "Merged" region in Figure 1.

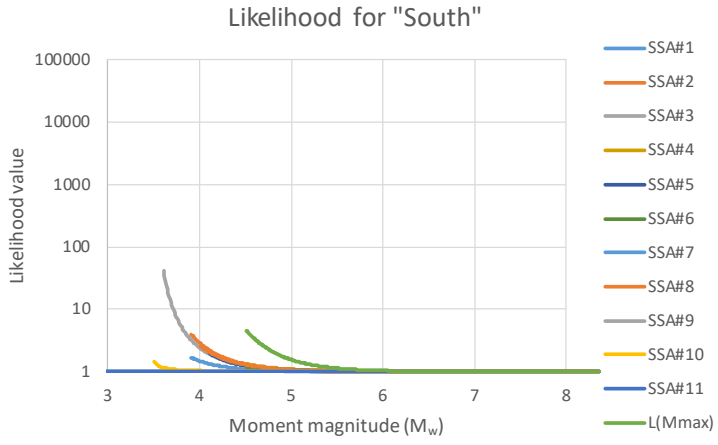

(a)

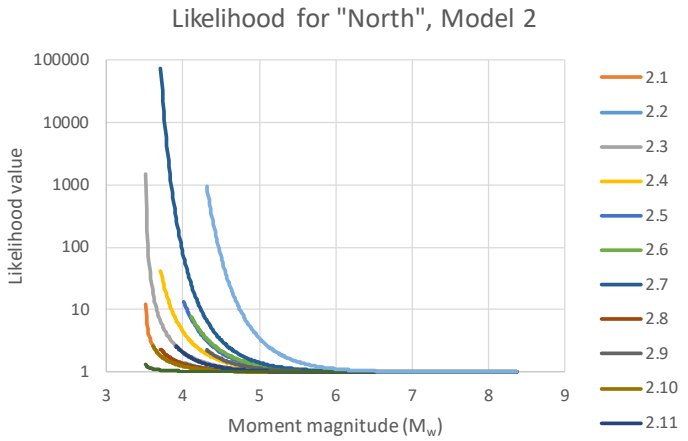

(b)

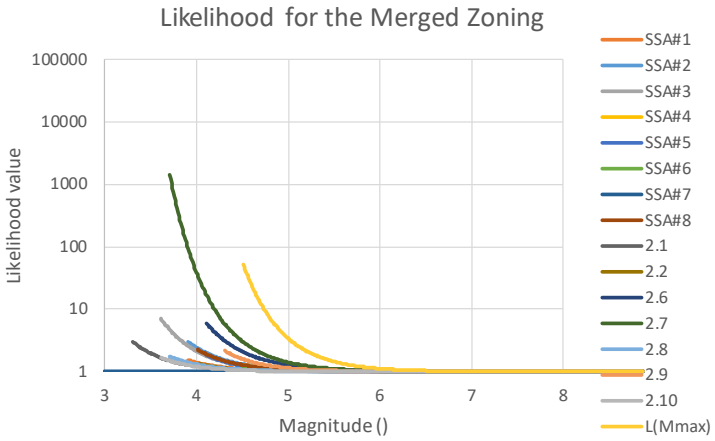

(c)

Figure 1. *Likelihood functions of individual SSA's in the regions (a) "South", (b) "North" and (c) merged for the entire Finland.*

The summarised likelihood function for all three regions are presented in Figure 2, compared to the initial estimates based on Table 1 input parameters.

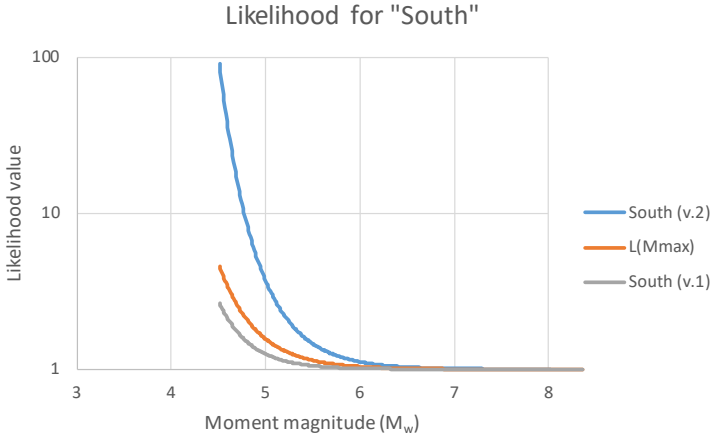

(a)

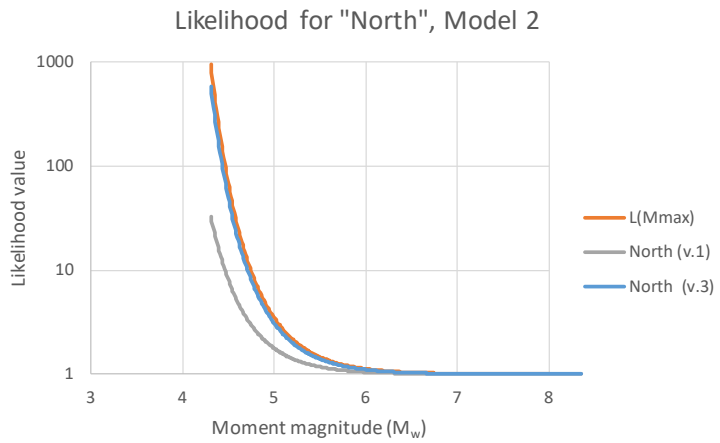

(b)

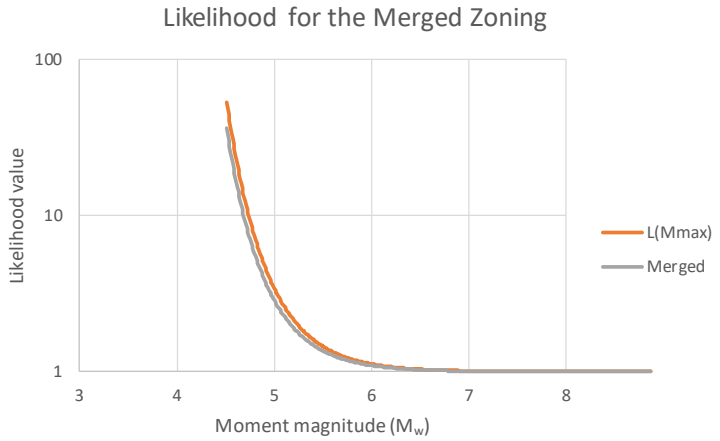

(c)

Figure 2. *Likelihood functions calculated with Equation 1 compared to the preliminary estimates based on parameters in Table 1, for regions (a) "South", (b) "North" and (c) "merged" for the entire Finland.*

- *Discussion*

It can be noticed that this method, more consistent with the completeness intervals of SSA's, will result with some changes of the likelihood functions. The biggest change occurs for region "South" (Figure 2a), where the updated completeness years are significantly shorter than the 517.98 years assumed in the preliminary calculations. With shorter observation interval the likelihood function drops, since the confidence of M_{max} being close to $M_{max,obs}$ is lower when the system was observed for shorter time.

The change is less significant in the region "North" and for the "merged" map (Figure 2.a &c), because the preliminarily used 131 years completeness is not very different from the newly estimated completeness values in Table 2 for SSA's of "North" Model 2.

The problem with this finding is that, since the likelihood function is not changing much from the preliminary values, we continue to have an M_{max} CDF from the Bayesian approach which is barely deviating from the CDF of the EPRI prior used (Figure 3). This may be interpreted in two ways. (a) The observed data in Fennoscandia (i.e. the likelihood function) is not sufficient and the Bayesian approach reverts to using the global M_{max} estimate for stable continental regions (i.e. the prior function). Or, (b) the observed data in Fennoscandia (i.e. the likelihood function) is basically incompatible with the used prior distribution, hence the outcome. There the two ways forwards with this:

(1) we accept the global SCR M_{max} estimate for Fennoscandia or

(2) we try to scrutinise if the prior distributing is suited for Fennoscandia.

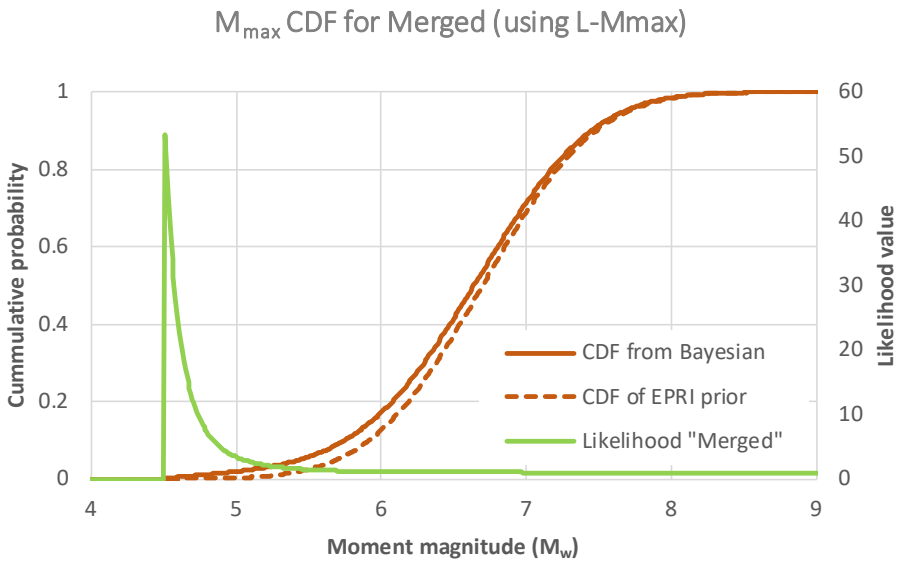

Figure 3. *Likelihood function of the merged region, CDF of M_{max} predicted by the Bayesian approach and the CDF's of the prior used (EPRI)*

The drawback for taking option (1) forward is that we later combine the Bayesian approach with the KSB approach. As shown in Figure 4, we are combining a method which suggest to use the M_{max} global SCR represented by the EPRI prior CDF, and a method that suggest with high confidence (α_0~1) that we should use a CDF not far from $M_{max,obs}$. Hence, we do not have a continuity of estimations, which we are sampling with the SENSEI M_{max} choice. We have an "*either-or*" scenario, with contradictory extreme estimates.

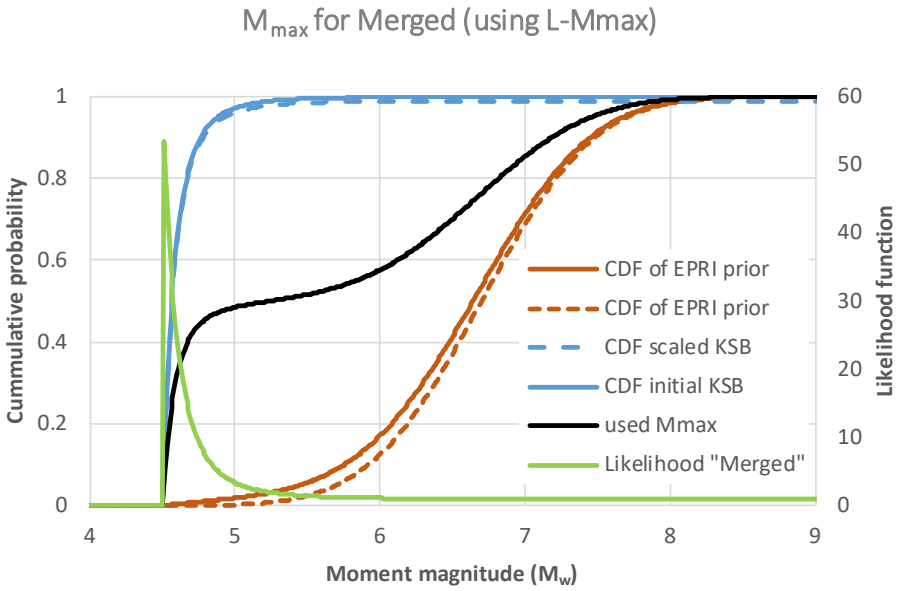

Figure 4. *Merged region, CDF's for M_{max} predicted by the Bayesian approach and by the KSB approach, and the "half-way between extremes" choice we could use in SENSEI*

The drawback of taking option (2) forward is that we do not know if we can achieve anything. There is argumentation in favour of using a single M_{max} estimate for all SCRs (e.g. Vanneste et al, 2016). This path could mean a stricter selection of the global seismological regions (e.g. perhaps narrowing the selection down to old shield regions) and the individual events (e.g. thinking if some SCR margins is relevant) feeding the data for the prior distribution definition. E.g. Ameri et al. (2015) applied the Bayesian approach for NPPs in France, and obtained a prior distribution compatible with the EPRI (1994) values (Table 3). At present we are using the NMESE version of EPRI (2012).

Table 3. Different prior distributions for the Bayesian method. The EPRI (1994) prior distributions were superseded by the EPRI (2012).

Prior	**mean M_w**	**STD M_w**
EPRI SCR (EPRI, 1994)	6.3	0.5
EPRI extended SCR (EPRI, 1994)	6.4	0.8
Non-Mesozoic and younger extension, NMESE (EPRI, 2012)	6.7	0.61
Mesozoic and younger extension, MESE (EPRI, 2012)	7.35	0.75
Composite, COMP (EPRI, 2012)	7.2	0.64
Ameri et al (2015) SCR part of Europe	6.2	0.5
Ameri et al (2015) active Europe (Italy, Greece etc.)	6.8	0.4

For instance, if a stricter scrutiny of the prior would result in a drop of 0.5 magnitude of the mean, we would end up with a M_{max} distribution like in Figure 5.

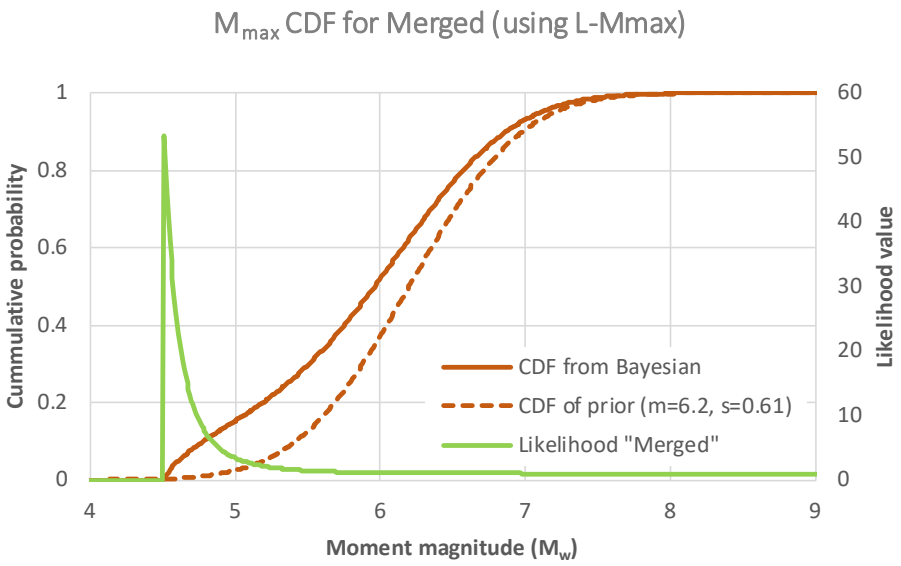

Figure 5. *Merged region, CDF's for M_{max} predicted by the Bayesian approach if a possible prior update (This is an example for what can be expected. Not a proposal in any way!)*

It would be probably more reasonable to use the Bayesian approach alone, with an updated prior than to mix the Bayesian and the KSB approaches, when they are evidently contradictory. The Bayesian approach with an updated prior would also likely result in a higher CDF than the combined Bayesian-KSB CDF we plan to use.

References

Ameri, G., Baumont, D., Gomes, C., Le Dortz, K., Le Goff, B., Martin C., Secanell R. (2015) On the choice of maximum earthquake magnitude for seismic hazard assessment in metropolitan France – insight from the Bayesian approach, 9ème Colloque National AFPS 2015 – IFSTTAR,

EPRI (2012), Central and Eastern United States Seismic Source Characterization for Nuclear Facilities. EPRI, Palo Alto, CA, U.S. DOE, and U.S. NRC: 2012.

EPRI (1994), The earthquakes of stable continental regions, Report EPRI TR102261

Korja, A., Kosonen, E. (Eds.) (2015). Seismotectonic framework and seismic source area models in Fennoscandia, northern Europe, Report S-63, Institute of Seismology, University of Helsinki, Helsinki, Finland.

Korja, A., Kihlman, S., Oinonen, K. (Eds.) (2016). Seismic source areas in central Fennoscandia, Report S-64, Institute of Seismology, University of Helsinki, Helsinki, Finland.

Vanneste K.; Vleminckx B.; Stein S.; Camelbeeck T. (2016), Could Mmax Be the Same for All Stable Continental Regions?, Seismological Research Letters (2016) 87 (5): 1214–1223. DOI: 10.1785/0220150203

Appendix 3.6 Arguments for a certain range of M_{min} in the PSHA sensitivity studies in Finland

L. Fülöp, P. Mäntyniemi, M. Malm, O. Kaisko / Espoo, 31.05.2019 – Draft 2 (*The purpose of this document is to supply structured background information to the expert group of the SENSEI project*)

Issue raised by expert group: **Line 21 in the SENSEI excel table**

"It is this reviewer's understanding that the PSHAs for Finnish NPPs used a minimum magnitude Mmin for the PSHA hazard integration that was equal to the Mmin used in the recurrence calculations (i.e., to obtain lambda and b [or beta]), and that these Mmin values ranged from 0.4 to 2.2. This is not standard practice in PSHA for nuclear facilities. As discussed by Bommer and Crowley (Seismological Research Letters, July/August 2017), the specification of Mmin for the PSHA integration is an engineering decision, not a seismological one. Mmin should be specified as the magnitude such that ground motions from earthquakes below that magnitude cannot cause damage to the structure or facility under consideration, regardless of the ground-motion amplitude. Mmin is typically set to Mw 5 for nuclear-plant PSHA, under the assumption that earthquakes with Mw<5 are incapable of damaging nuclear structures. This value is based largely on modeling and observations contained in EPRI Report NP-6389 (1989)."

Suggested resolution by expert group

*"Perform PSHA calculations using Mmin=4 (as a sensitivity calculation) and 5 (recommended value) for all source zones. Caution, if the rates entered as input to EZ-FRISK are the rates of earthquakes above Mmin, then the rates for the new Mmin must be calculated and entered [this should be confirmed by careful reading of the EZ-FRISK documentation]. The equation to use is lambda(>Mmin_PSHA)=lambda(>Mmin_recurrence)*exp(-beta*(Mmin_PSHA - Mmin_recurrence)). Note: choosing Mmin=4 or 5 will remove the need to have GMPEs that predict ground motions for very low magnitudes."*

Introduction / Background

The minimum magnitude for the hazard integration M_{min} is an important parameter of the PSHA models. In the integral formulation the probability of exceeding a level of an intensity measure (IM) from a single source is written as.

$$P(\mathrm{IM} > x) = \int_{M_{min}}^{M_{max}} \int_{0}^{r_{max}} P\,(\mathrm{IM} > x|m,r) f_M(m) f_R(r) dr dm \qquad (1)$$

In Eq. (1) $f_M(m)$ and $f_R(r)$ are the probability density functions of the magnitude and distance distribution of earthquakes, respectively. In practical calculations, the continuous integrals are computed with discrete summations. The limits of integration can be chosen as follows; r_{min}=0 means that the hazard summation starts from the site (r_{min}=0 may also imply that the site is located within the source zone); r_{max} is the distance from the site from where no earthquake is expected to pose a significant risk to the site, extending r_{max} will have a negligible effect on the hazard at the site; M_{max} is the magnitude of the largest earthquake expected within the source zone. M_{max} should exceed the largest observed magnitude within the source zone, and its value can be established using geological arguments or statistical analysis of earthquake observations. On the other hand, M_{min} should be

established from engineering considerations regarding the fragility of the installation at the site. Specifically, earthquakes below M_{min} are considered not to pose a risk to the NPP installations.

The calculation issue with the integration limits is that all quantities within the integral should be defined between the limits of R_{min} to R_{max} and M_{min} to M_{max}. Particularly, $f_M(m)$ which is based on the activity rates need a definition, down to M_{min} and up to M_{max}. This issue leads to argument about the completeness of the earthquake catalogue in different historic times, characterised by different magnitude thresholds M_{th} of detecting earthquakes. On the other side, the $f_M(m)$ function is, by definition, based on extrapolation to M_{max}.
The presence of extended sea areas within a source zone may also hinder observation of earthquakes, hence potentially affecting both $f_M(m)$ and $f_R(r)$. Before the instrumental era, the likelihood of an earthquake being felt in populated regions is higher. In the case of Finland, both earthquakes with epicentres in sea areas, or within the sparsely populated inland regions may remain unrecorded.

In addition, a definition for $P(\mathrm{IM} > x|m,r)$, which requires information on the attenuation rate, typically in terms of the GMPE, also needs a definition for the entire range of R_{min} to R_{max} and M_{min} to M_{max}. This poses a limitation especially in terms of M_{min}, since international GMPEs transferred from regions with higher seismicity, are often valid from a high M_{min}, in relation to the seismic activities in Fennoscandia.

Backgrounds of the PSHA calculation in Finland

In the latest PSHA studies, the M_{min} used was different for each source zone, and was equal to the catalogue completeness limit M_{th}. The careful determination of M_{th} for different source zones and their respective subcatalogues, including recent times with low magnitude thresholds for complete earthquake recording, is an issue in a low-seismicity region such as Fennoscandia, because of the need to broaden the available magnitude ranges for the estimation of the *b* value. Typically, zone-specific *b* values have been estimated. As a rule of thumb, data extending over at least 3 orders of magnitude provide a reasonable basis for the estimation of the *b* value. Methods describing the incorporation of subcatalogues with different time spans and different thresholds M_{th} can be found in the literature: in particular, Weichert (1980) and Kijko and Sellevoll (1989, 1992) dealt with this topic. The determination of the thresholds for complete recording is avoided only if a global *b* value is assumed (cf. SHARE project).

Choosing M_{min} to correspond M_{th} poses a potential problem for PSHA calculation, because the GMPEs also need a definition down to this M_{min}. Such GMPEs are not readily available in the international literature. The Fennoscandian GMPE utilizing the local recordings has been introduced down to magnitude 1.0 (Vuorinen et al., 2017) and updated in Report T-97. The T-97 GMPE was the basis of the FENNO PSHA calculations.

In earlier hazard study made for STUK (Saari et al., 2009), and the SESA project (Fülöp et al, 2015) M_{min}=2 has been used. It should be noted that the attenuation tables of the GMPE in those studies (i.e the same Varpasuo *et al*. 2000 use at LO and OL) start from magnitude M2.5.

Possible basis for selecting M_{min}

1. Fragility of the plant buildings and equipment

Appendix 3.6

US NPPs had a safe shutdown earthquake (SSE) as basis of their design. The SSE horizontal PGA values are listed in Table 1. These PGAs were used together with the RG 1.6 or similar generic spectra for engineering characterization of large magnitude earthquakes, to design the plants. The horizontal PGA was often supplemented with vertical component.

For the US conditions, EPRI (1989) argues that: "*For NPPs designed and constructed to withstand broad-band spectra representative (sic) large earthquake motion, it is reasonable to accept that there is a minimum magnitude below which there is reasonable engineering assurance that damage for smaller events is negligible*". Based on experience data and a wide agreement among US earthquake engineers, the threshold of small events is placed at M5.0 by EPRI (1989).

Table 1. Summary of the original SSE spectral shape for the US plants (OECD, 2019)

Name	Horiz. SSE PGA (g)	Name	Horiz. SSE PGA (g)	Name	Horiz. SSE PGA (g)
Arkansas Nuclear	0.2	Enrico Fermi 2	0.15	Peach Bottom 2, 3	0.12
Arkansas Nuclear	0.2	James A. FitzPatrick	0.15	Perry	0.15
Beaver Valley 1	0.125	Fort Calhoun 1	0.17	Pilgrim 1	0.15
Beaver Valley 2	0.125	Ginna	0.2	Point Beach 1, 2	0.12
Braidwood 1, 2	0.2	Grand Gulf	0.15	Prairie Island 1, 2	0.12
Browns Ferry 1, 2, 3	0.2	Shearon Harris	0.15	Quad Cities 1, 2	0.24
Brunswick 1, 2	0.16	Edwin I. Hatch 1	0.1	River Bend	0.1
Byron 1, 2	0.2	Edwin I. Hatch 2	0.15	H.B. Robinson	0.2
Callaway	0.2	Hope Creek	0.2	St. Lucie	0.1
Calvert Cliffs 1, 2	0.15	Indian Point 2, 3	0.15	Salem 1, 2	0.2
Catawba 1, 2	0.15	LaSalle County 1, 2	0.2	Seabrook Station	0.25
Clinton	0.25	Limerick 1, 2	0.15	Sequoyah 1, 2	0.17
Columbia	0.23	McGuire 1, 2	0.15	South Texas 1, 2	0.1
Comanche Peak 1, 2	0.12	Millstone 2	0.17	Virgil C. Summer	0.15
Donald C. Cook 1, 2	0.2	Millstone 3	0.17	Surry 1, 2	0.15
Cooper	0.2	Monticello	0.12	Susquehanna 1,2	0.1
Davis-Besse	0.15	Nine Mile Point 1	0.13	Three Mile Island 1	0.12
Diablo Canyon	0.8	Nine Mile Point 2	0.15	Turkey Point 3, 4	0.15
Dresden 2, 3	0.2	North Anna 1, 2	0.12	Vogtle 1, 2	0.2
Duane Arnold	0.12	Oconee 1, 2, 3	0.1	Waterford 3	0.1
Oyster Creek	0.18	Palisades	0.2	Watts Bar 1, 2	0.18
Joseph M. Farley	0.1	Palo Verde 1, 2, 3	0.19	Wolf Creek	0.15

In Finland, none of the NPPs with the exception of the recently finished OL3 have been designed for any earthquake loads when constructed. Hence, the basic premise of EPRI (1989) is not fulfilled. However, NPPs in Finland have been built using the structurally resilient cast-in-situ technique.

A refined approach for establishing M_{min} could follow Bommer & Crowley (2017). They argue that M_{min} is "*an engineering parameter that is ultimately related to seismic risk rather than seismic hazard*". They also state that "*the confusion surrounding the M_{min} topic could be alleviated by defining lower limits on appropriate intensity measures rather than on magnitudes used as a proxy for shaking levels*". Such lower limit in intensity measures (IMs like e.g. PGA, SA etc.) should results from the fragility values of components in Finnish plants.

Fragility analysis of has been carried out (Varpasuo 1996) and updated periodically. The table below summarises the fragility parameters of LO components with $HCLPF_{PGA}$ of less than 0.15g. Some components have low $HCLPF_{PGA}$ and low median capacity (A_m) and in some cases the low $HCLPF_{PGA}$ is due to uncertainty (β). Additional 11 components have $HCLPF_{PGA}$ between 0.15-0.2g.

Table 2. Fragility parameters for LO components (Varpasuo, 1996)

Component description	Component. designator	Building	Elevation	A_m (g)	β_R	β_U	$HCLPF_{PGA}$(g)
Feedwater tank	RL10B001	Turbine	+19.8M	0.15	0.28	0.38	0.050
Deionization tank	RVOIBOOI	Yard	Grade	0.16	0.25	0.25	0.070
RHR heat exchanger	RR21WO01	Turbine	+3M	0.3	0.44	0.44	0.070
EFW pumps tub. tank	VG20BOOl	Turbine	+20M	0.31	0.27	0.39	0.104
Steam generator	YB11	Reactor	-	0.4	0.28	0.53	0.105
Components cooling exp. Tank	TF60BOOl	Aux Bldg	22M	0.45	0.38	0.35	0.135
Field flash batteries	IEC20	D/G	+3.8M	0.47	0.38	0.35	0.141
Station emergency batteries	IEC03	Lab	+3M	0.47	0.38	0.35	0.141
Monitors on benchboard	GA	Control	13.8M	0.5	0.38	0.35	0.150
Offsite power	AC, AE	Yard	Grade	0.3	0.22	0.2	0.150

The seismic PRA for LO was updated by Helander and Jänkälä (2012). In their calculations the previously weakest feed-water tank and deionization tank have upgraded median capacity (A_m's). However, two steam generators were estimated to have lower median capacity.

Table 3. Updated fragility parameters for LO components (Helander and Jänkälä, 2012)

Component group	Kz	A_m (g)	β_R	β_U	$HCLPF_{PGA}$(g)
Steam generators YB11/15/56	YB11/15/56W01	0.17	0.28	0.38	0.057
Steam generators YB13/52/54	YB13/52/54W01	0.23	0.28	0.38	0.077
RHR heat exchangers	RR21/22W01	0.36	0.44	0.44	0.084
Feed water tanks	RL10/50B01	0.28	0.28	0.38	0.094
Deionization tanks	RV01/03B01	0.24	0.25	0.25	0.105
Demineral water tanks	TD51-53B01	0.24	0.25	0.25	0.105

LPSI accumulators	TH40/80B01/02	0.39	0.28	0.38	0.131
Control room monitors	GA	0.47	0.38	0.35	0.141
Power substation	AC/AE	0.3	0.22	0.2	0.150

The failure modes listed in Table 2 and Table 3 are mostly mechanical failure of e.g., anchors. Hence, they may have very different damage resilience to large distance shaking and near-field single pulls type loading, even when the two have the same intensity (e.g., PGA). However, this issue relates to the inadequacy of the PGA as intensity measure (IM) in fragility calculations (*especially in Finland because of the hard-rock and the complete lack of larger earthquakes at some distance?!*).

It does not seem appropriate to solve the inadequacy of IM by lowering the hazard, by dropping from the integral earthquakes that produce short pulls-like ground motion. Instead, earthquakes that are capable to produce PGAs in the ranges interacting with the above fragilities should be included in the hazard integral.

2. Indications for deaggregation of the hazard

In the SESA project, deaggregation of the hazard have been published for the PGA, SA_{4Hz} and SA_{10Hz}, of significance for Finnish NPPs (i.e. PGA>0.05g and associated SA's). These plots are based on some of the areal source zones of Saari and others (2009) and the VNS (Varpasuo-Nikkari-Saari) GMPE (Varpasuo et al., 2000), hence they are not entirely relevant today. However, with diffuse seismicity in Finland, it can be expected that the trends are not very different for different sites. We deaggregated SA_{4Hz} as a proxy for frequency range relevant to NPP buildings and SA_{10Hz} as a proxy for NPP equipment. The plots ere reproduced below for the location of Pyhäjoki:

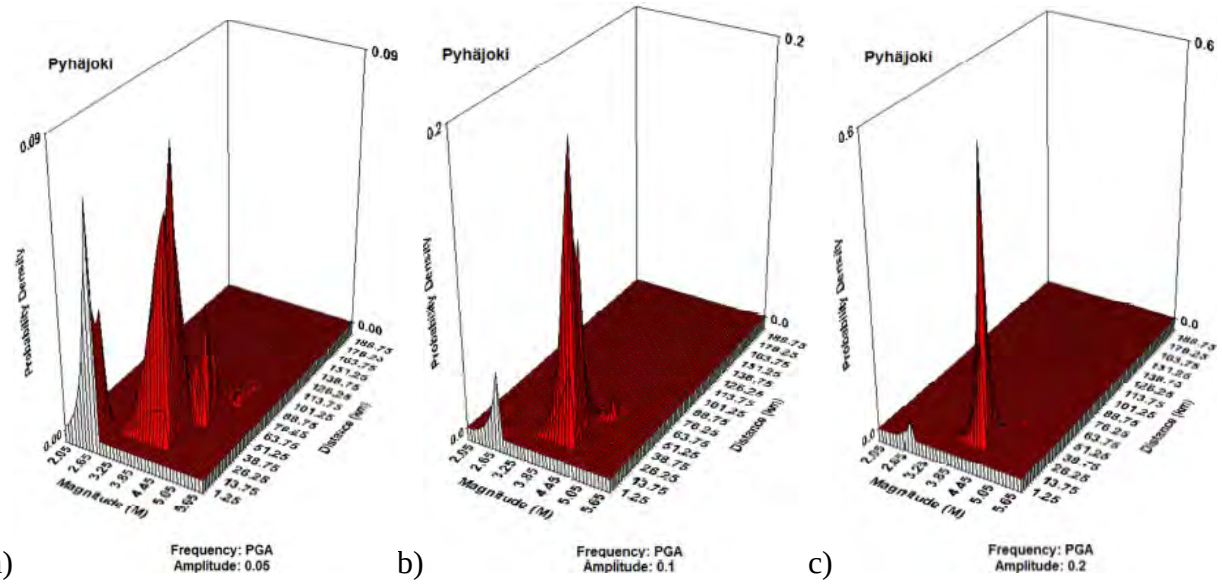

a) b) c)

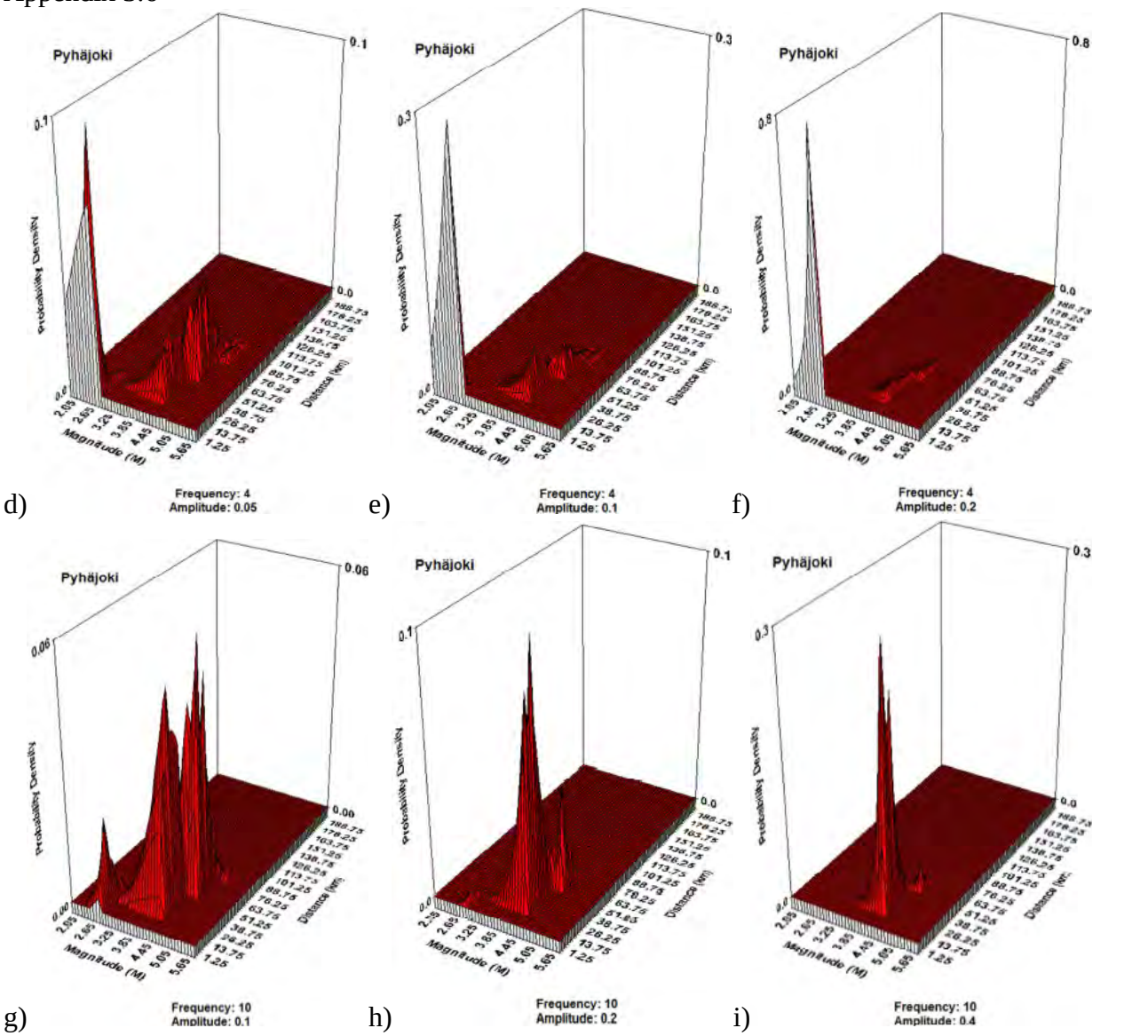

d) e) f)

g) h) i)

Figure 1. *EZ-FRISK magnitude-distance de-aggregation for Pyhäjoki, 5 % damping, average horizontal component of PGA amplitude (a) 0.05g, (b) 0.1g, (c) 0.2g; 4Hz spectral amplitude for (d) 0.05g, (e) 0.1g, (f) 0.2g; and 10Hz spectral amplitude for (g) 0.1g, (h) 0.2g and (i) 0.4g.*

It can be noticed that the M_{min} used in this study was M2, hence there is a cut-off for the plots at M2. This cut-off is affecting the hazard only for SA_{4Hz}, where significant part of the plot is tapered.

The largest extent of the deaggregation peaks at the higher end of M's is controlled by the M_{max}. In this study M_{max} was source zone dependent with values of M_{max}=3.0 (Central Finland Quiet Zone) and M_{max}=4.6 (Southern Bothnian Bay – Ladoga Zone) for the source zones closest to the site. Increased M_{max} will extend the deaggregation peaks both towards higher M's and larger distances.

In the SA_{4Hz} plots, it appears that very close-range small earthquakes (M<2.5, R_{epi}<10km) are potential sources of hazard, together with M>3 and R_{epi}~10…100km. For SA_{10Hz} plots lack the M<2 peaks, they are in the range M>3 and R_{epi}~10…100km. The PGA plots are also concentrated in M>3 and R_{epi}~10…100km. The peaks at magnitudes below 3 vanish with increasing amplitude, which is reasonable.

We can safely assume that M~2.5 earthquake do not pose risk to NPP buildings and ignore the first peaks in Figure 1def. The same argument is more difficult to make for NPP equipment (Figure 1g, 1h, 1i). Hence, a possible M_{min} could be ~M3…M3.5, in order not to taper the de-aggregation peaks in Figure 1g, 1h, and 1i. If we choose ~M4, part of the hazard would be ignored in the PSHA computation, solely based on the postulated assumption that M3-M4 does not pose a risk to plant equipment.

3. Indications from the ranges of M_{max} used in Finnish PSHA studies

Three of the most recent PSHA studies done in Finland (Hanhikivi, Olkiluoto, and Loviisa) have all used the same maximum magnitudes in the computations: 5.5, 6.0, 6.5, and 7.0 (Saari et al., 2015; Saari & Malm, 2016; Malm & Kaisko, 2017a&b). Also, the weights of the logic tree branches for these maximum magnitudes have been of the same order. Earlier studies have used the maximum observed magnitude for the source area or region +0.1 or +0.5 -approach.

Table 4. Summary The ranges of Mmax and the branch weights used in the logic trees of recent PSHA studies in Finland.

Site	**Study**	**M_{max} used in logic tree (weight for the branch)**
Pyhäjoki, Simo, Gridpoint C, Gridpoint E (STUK)	Saari et al., 2009	max. observed for source area or region +0.1 (0.5) max. observed for source area or region +0.5 (0.5) Pyhäjoki catalogue max. observed 3.0 – 5.2 Simo catalogue max. observed 3.0 – 5.8
Hanhikivi (Fennovoima)	Saari et al., 2015; Malm & Kaisko, 2017a	5.5 (0.70), 6.0 (0.22), 6.5 (0.06), 7.0 (0.02)
Olkiluoto (TVO)	Saari & Malm, 2016; Malm & Kaisko, 2017b	5.5 (0.72), 6.0 (0.21), 6.5 (0.06), 7.0 (0.01)
Loviisa (Fortum)	Saari & Malm, 2016; Malm & Kaisko, 2017b	5.5 (0.70), 6.0 (0.22), 6.5 (0.06), 7.0 (0.02)

4. Indications from international comparisons

In the CompPSHA study we collected information on the minimum cut-off magnitude considered in different countries (M_{min}). In addition, the M_{max} in the earthquake catalogues was reported. Unfortunately, the M_{max} is not connected to any distance information between the M_{max} event and the site. The PGA for the current licensing basis was also provided by the responders. This value is not identical to the SSE in US terminology, instead it should take into account all the upgrades that of the plant.

Table 5. Summary The ranges of Mmax and the branch weights used in the logic trees of recent PSHA studies in Finland.

	M_{min}	M_{max} in the earthquake catalogue	Current PGA(g) free-field
Belgium	5	6.3	0.1-0.17
Finland	*2-2.5*	*5.8*	*0.1-0.2*
France	5	5.9	0.1-0.2
Germany	Not stated	6.6	0.05-0.21

Japan	No significant effect on the hazard	9	
Netherlands	-	*6.6*	*0.06*
Korea	5	-	0.2-0.3
Spain	*3.5 for IPEEEs***	*8.2*	*0.1-0.2*
Sweden	*NA*	*6*	*0.11*
Switzerland	4.5	6.6	0.4-0.5

*Individual Plant Examination of External Events

The M_{min} is reported not to influence significantly the hazard results in Japan due to the abundance of the mid-size earthquakes (OECD, 2019). Several low seismicity countries do not report M_{min}. Both the catalogue M_{max} and M_{min} are the smallest in Finland, with the reported maximum observed M5.8 belonging to the Lurøy earthquake located on the coast of Nordland, Norway. It is the largest onshore/nearshore earthquake in the historical seismicity record of Fennoscandia.

It is not possible to suggest M_{min}, based on these comparisons. As highlighted by Bommer & Crowley (2017) M_{min} should have no connection to the seismicity of a region. Of course, an indirect connection exists; the industry in countries with very small seismicity do not have the tradition to design and build earthquake resilient buildings. Hence, one can expect higher vulnerability in such countries.

Suggested ranges of M_{min}

The basis for choosing M_{min} should be the fragility of the plant buildings and equipment. The other information is given as auxiliary/supporting information.

References

Bommer, J.J., Crowley, H., 2017. The Purpose and Definition of the Minimum Magnitude Limit in PSHA Calculations. Seismological Research Letters 88, 1097–1106. https://doi.org/10.1785/0220170015

EPRI, 1989. Proceedings: Engineering Characterization of Small-Magnitude Earthquakes, NP-6389

Fülöp, L., Jussila, V., Malm, M., Tiira, T., Saari, J., Li, Y., Mäntyniemi, P., Heikkinen, P., Puttonen, J., 2015. Seismic Safety of Nuclear Power Plants - Targets for Research and Education (SESA) - Final Report, in: SAFIR2014, The Finnish Research Programme on Nuclear Power Plant Safety 2011-2014, (Final Report), VTT Technology. VTT Technical Research Centre of Finland, Espoo, pp. 604–619.

Helander J. and Jänkälä K, (2012), The Update of Seismic Probabilistic Risk Analysis for Loviisa Nuclear Power Plant, International Probabilistic Safety Assessment and Management Conference and Annual European Safety and Reliability Conference (PSAM11and ESREL 2012); ISBN: 978-1-62276-436-5 (https://www.iapsam.org/www.psam11.org/www/fi/papers/index.php.html)

Malm, M. and Kaisko, O., 2017a. Updated ground response spectrum for the Hanhikivi site, Report DFVUDBR-5638, ÅF-Consult Ltd, 6 pp. Espoo, Finland

Malm, M. & Kaisko, O., 2017b. Re-evaluation of seismic hazard spectra in Olkiluoto and Loviisa, ÅF-Consult Ltd, Report DTVOSPF-5497, 19 pp. Espoo, FinlandSaari, J., Heikkinen, P., Varpasuo, P., Malm, M., Turunen, E., Karkkulainen, K., Valtonen, O., Uski, M., 2009. Estimation of Seismic Hazard in Territory of Finland (No. Report Number EXP-500). ÅF-Consult.

Saari, J., Lund, B. Malm, M., Mäntyniemi, P., Oinonen, K., Tiira, T., Uski, M., Vuorinen, T., 2015. Evaluating Seismic Hazard for the Hanhikivi Nuclear Power Plant Site, Seismological Characteristics of the Seismic Sorce Areas, Attenuation of Seismic Signal, and Probabilistic Analysis of Seismic Hazard, ÅF-Consult Ltd, Report NE-4459, Espoo, Finland.

Saari, J. & Malm, M., 2016. Re-evaluation of seismic hazard in Olkiluoto and Loviisa, ÅF-Consult Ltd, Report DTVOHAR-4652, 25 pp. Espoo, Finland.

Varpasuo, P., Puttonen, J., Ravindra, M.K., 1996. Seismic probabilistic safety analysis of unit 1 of the Loviisa nuclear power plant. Nuclear Engineering and Design 160, 411–426. https://doi.org/10.1016/0029-5493(95)01118-8

Varpasuo, P., Nikkari, Y. and Saari., J. 2000. Estimation of seismic hazard in territory of southern Finland, Fortum Engineering Ltd. Report LVOI-A6-951M2

Appendix 3.7 Comparative plots of GMPEs

L. Fülöp / Espoo, 29.08.2019 – Draft 2 (*The purpose of this document is to supply structured background information to the expert group of the SENSEI project*)

Issue raised by expert group: **Line 23 in the SENSEI excel table**
"In case two published GMPEs have to be combined in a single model (because they apply to different magnitude ranges, for instance) a sensible transition between the two models has to be warranted. PSHA results (in particular, the strange shape of the UHS) together with discussion during the meeting in Helsinki (March 5th-6th) suggests that this is not the case. This point was raised during the Helsinki meeting, however, according to what it was spoken during the latest teleconference (April 3rd) and also according to comment by G. Toro in line #20 above, this comment may become non-applicable. In any case, since it was discussed, it is included here.

Suggested resolution by expert group
"Firstly, the equivalence of parameters handled by the two GMPEs has to be checked: this applies mainly to type of magnitude, type of distance and type of ground motion being provided (i.e., geometric mean or other).
Once the previous homogeneity has been proven or achieved, visual inspections of plots coming from the two GMPEs is to be conducted in order to see if a transition if possible and if affirmative, propose the type of transition that seems logical."

Backgrounds to the GMPEs in the comparisons

The GMPEs in these comparisons are the ones used in Finland in recent studies, the ones developed for Fennoscandia and the ones suggested for consideration in the SENSEI meetings by the Expert Group. It is considerable effort to implement and check a GMPE from a publication, so we concentrated on the ones strongly suggested for consideration by the Experts Group.

The intention was to plot the GMPEs covering the entire range of interest for the different PSHA studies, approximately: M_w2-7, R0-300km, depth 0-30km, frequency 1-100Hz. These ranges may change as the SENSEI project advances, and in some cases, we anticipated this change. E.g., in recent PSHA studies magnitudes below M_w2 were included, but we do not plot GMPEs in that range, anticipating that the M_{min} will be raised even above M_w2.

The plotted GMPES are:

- The GMPE developed by Varpasuo *et al* (2000) and updated by Leppanen and Varpasuo (2017). This GMPE, called VSN or VNS 2017 here, was the basis for the Loviisa and the Olkiluoto PSHA study received by the SENSEI project group from STUK.
- The corrected New Fennoscandian GMPE described in Report T-97 of the Institute or Seismology (Vuorinen *et al*, 2018). This GMPE was the basis for the Hanhikivi study received by the SENSEI project group.
- The Pezeshk et al (2011) model, which was the basis for developing the T-97 GMPE.
- The Fenno-G16 GMPE developed in the SAFIR EVOGY project (Fülöp *et al*, 2019). This GMPE is recent and has not been used in PSHA studies.
- The G16 GMPE by Graizer (2016), which was the basis of the Fenno-G16 model.
- The NGA-East GMPE family published by PEER (Goulet *et al*, 2018).

Appendix 3.7

Comparative plots of GMPEs in the application range for PSHA models in Finland

The following comparisons are made:

- **Annex A:** All GMPEs used in Finland earlier (VNS and T-97) + Pezeshk + G16 + FennoG16 + Si et al. (suggested by Timo in the last Expert Group meeting) are compared among themselves. Range is magnitudes M3, M5 and M7; frequencies PGA, 25Hz, 10Hz, 5hz and 1Hz, distance up to 300km. Because the VNS GMPE used for OL and LO is in fact a family of four GMPE's, only one (Saguenay Longitudinal) is plotted. Hypocentre depths are h=5km and h=30km in the upper and lower plot.
- **Annex B:** The four GMPEs within VNS is plotted to compare to each other. Same ranges as above. Hypocentre depths are h=5km and h=30km in the upper and lower plot.
- **Annex C:** G16 and FennoG16 are compared to all NGA-East GMPEs. This was done by plotting over some existing figures of the NGA-East GMPEs, so the ranges are different. Magnitude M4.5, 5.5, 6.5 and 7.5. Distances are 20, 50, 100 and 200km. The entre spectra is plotted between ~1Hz and 100Hz.
- **Annex D:** Plots of all GMPEs (as in Annex A) compared with some earthquake recordings. M2.4 and M3.1 are Fennoscandian events. All other are Canadian earthquakes with reported Vs=2000m/s and data included in the NGA East dataset. Plotting magnitude and depth as given for the earthquake.
- **Annex E:** Same data comparison plots, but only for the four VNS 2017 GMPEs.

Observations

Since the complete range of interest from PSHA point of view is plotted, we can observe trends that may result in spurious hazard values from a specific range, but we can also observe ranges of compatibility between GMPEs. These ranges of compatibility can be used to provide "a *sensible transition between the two models"*. Observations and suggestions are as follows.

The VSN (2017) GMPE has a dual behaviour; the different components give very different prediction (e.g., Annex B). When we compare to data some components are reasonable (the Saguenay based components), but others significantly under predicts the ground motion (Annex E). If we consider that Finnish PSHA studies output median hazard, the outcomes with VSN (2017) largely depend on the weights associated to the different branches of the GMPE components. In the PSHA models the Saguenay branches were weighted 60% and the Newcastle branches 40%. Hence, the median hazard was probably based on the Saguenay branches and was reasonable.

The T-97 GMPE compares reasonably with other GMPEs (Annex A) and data (Annex D), except for lower frequencies, starting already at 5Hz. The T-97 prediction is bad at 1Hz, but the GMPE is not recommended for 1Hz by its developers and has not been used in the Hanhikivi PSHA at 1Hz. Instead, the Pezeshk GMPE was employed at 1Hz and 5Hz and the T-97 model for higher frequencies. The large gap between the two GMPEs at 5Hz (Annex A) is a probable explanation for the drop in the Hanhikivi hazard in this frequency.

Fenno-G16 compares reasonably with other GMPEs (Annex A) and data (Annex D). It also compares reasonably in a broad frequency range with the NGA-East GMPE family magnitudes up to M_w6 (Annex C). It is aligned with the higher predictions in the NGA-East set of 17 GMPEs, especially for the spectral peak prediction. The precision drops at M_w7 for frequencies below 1Hz. Fenno-G16 could reasonably be used for frequencies above 1Hz.

The good match between Fenno-G16 and the NGA-East set at M_w4-5also offers the possibility to swap GMPE at this magnitude range. Hence, a PHSA model could use Fenno-G16 for magnitudes lower than e.g., M_w5 and NGA-East model(s) for M_w>5 up to M_w8.2.

Attenuation tables for the NGA-East 17 components, for the NGA-East weighted mean GMPE, Fenno-G16, T-97 and VSN 2017 were prepared for the project.

References

Fülöp, L., Jussila, V., Aapasuo, R., Vuorinen, T., Mäntyniemi, P., 2019. Evolving the Fennoscandian GMPEs (EVOGY). SAFIR2018 - The Finnish Research Programme on Nuclear power Plant Safety 2015-2018: Final report 422–433. https://doi.org/10.32040/2242-122X.2019.T349

Goulet, C.A., Yousef, B., Ancheta, T.D., Norman, A., Nicolas, K., Linda, A.A., Robert, Y., Robert, G., Gail, A., 2018. Central and Eastern North America Ground-Motion Characterization NGA-East Final Report (No. PEER 2018/08). Pacific Earthquake Engineering Research Center, California, Berkeley.

Graizer, V., 2016. Ground-Motion Prediction Equations for Central and Eastern North America. Bulletin of the Seismological Society of America 106, 1600–1612. https://doi.org/10.1785/0120150374

Leppänen, T., Varpasuo, P., 2017. Loviisa 1 ja 2, Olkiluoto - Loviisa NPP sites , ground motion prediction equations (No. LO1-T84252- 00005, Version 1). Fortum Power and Heat O.

Pezeshk, S., Zandieh, A., Tavakoli, B., 2011. Hybrid Empirical Ground-Motion Prediction Equations for Eastern North America Using NGA Models and Updated Seismological Parameters. Bulletin of the Seismological Society of America 101, 1859–1870. https://doi.org/10.1785/0120100144

Varpasuo, P., Nikkari, Y. and Saari., J. 2000. Estimation of seismic hazard in territory of southern Finland, Fortum Engineering Ltd. Report LVOI-A6-951M2

Vuorinen, T., Tiira, T., Uski, M., Lund, B., 2018. Updated Fennoscandian GMPE (No. Raport T-97). Helsinki University, Institute of Seismology, Helsinki, Finland.

Appendix 3.7

Annex A: Compare_All GMPEs

	PGA	25Hz	10Hz	5Hz	1Hz
M_w=3	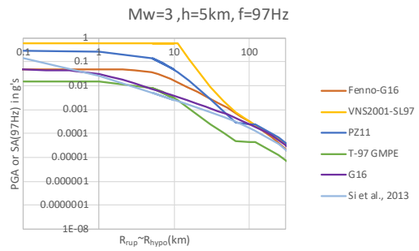	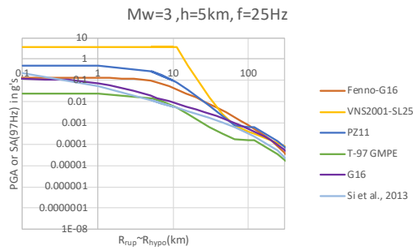	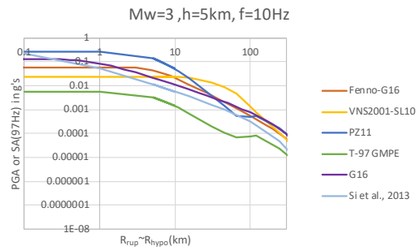	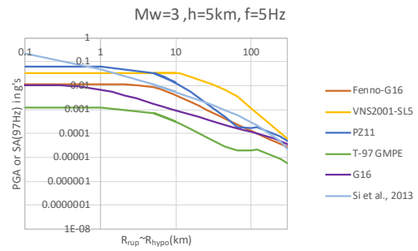	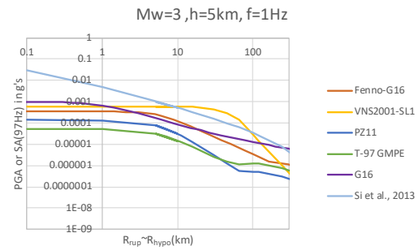
M_w=5	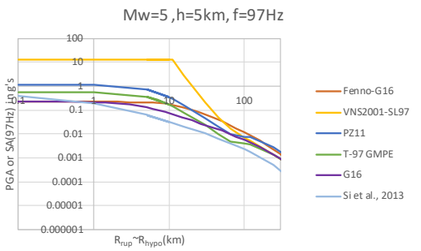	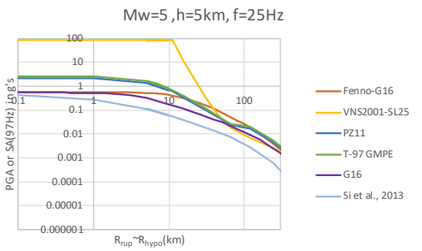	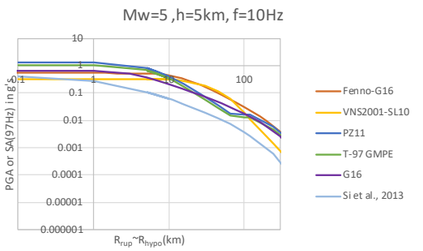	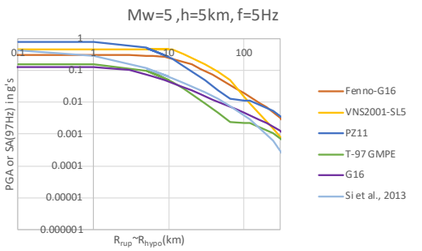	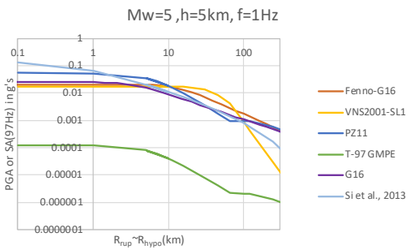
M_w=7	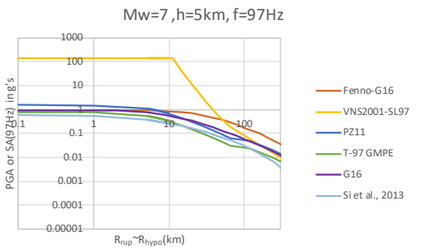	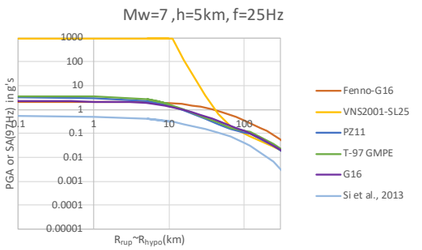	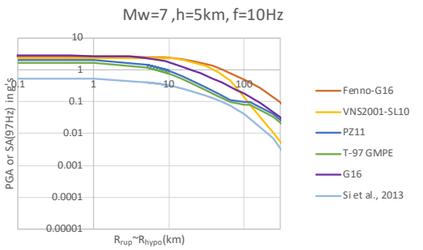	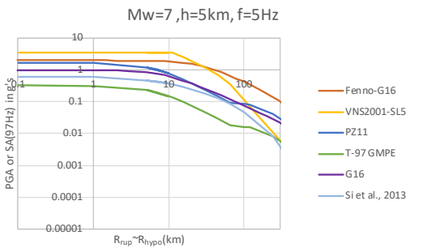	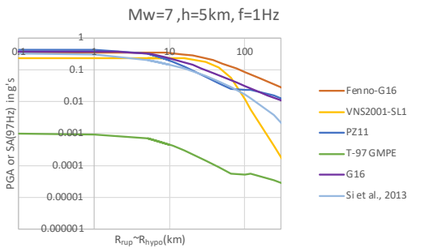
M_w=3	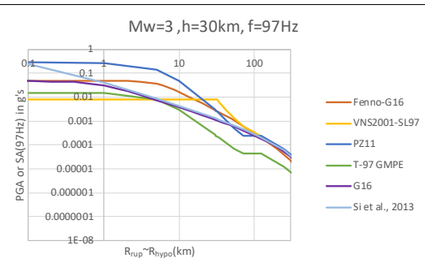	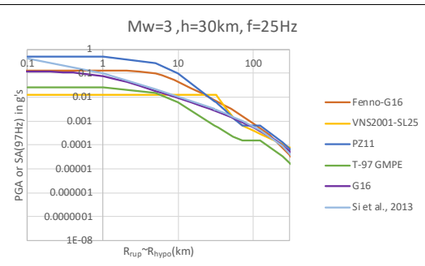	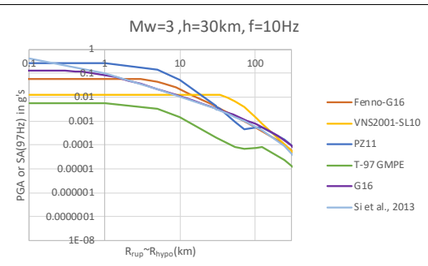	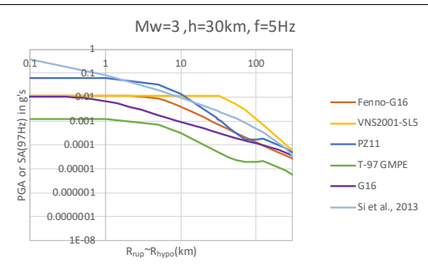	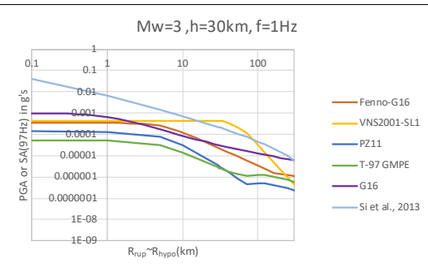
M_w=5	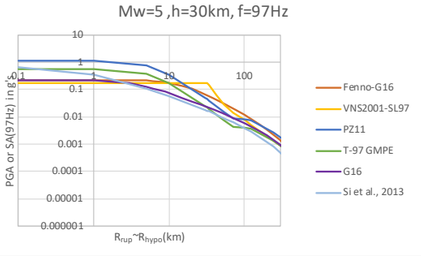	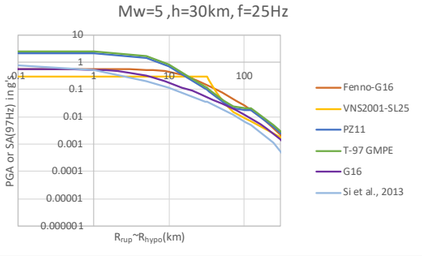	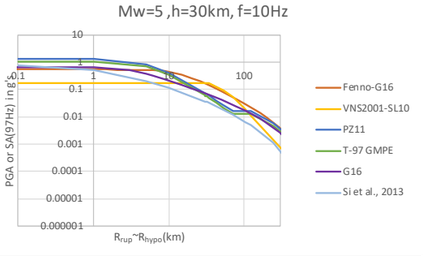	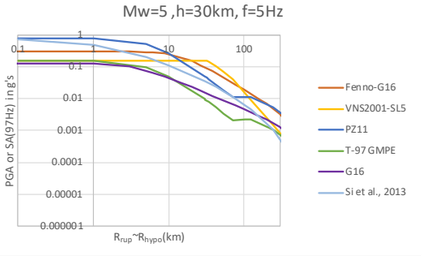	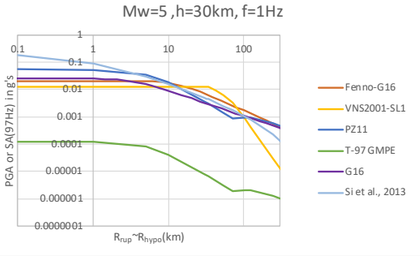
M_w=7	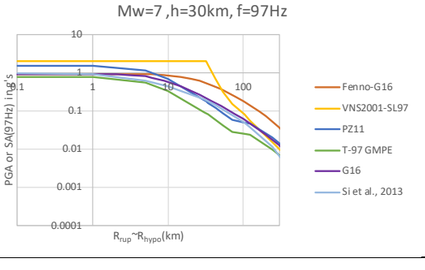	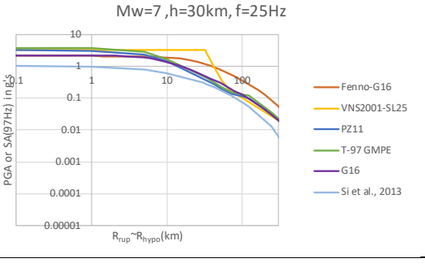	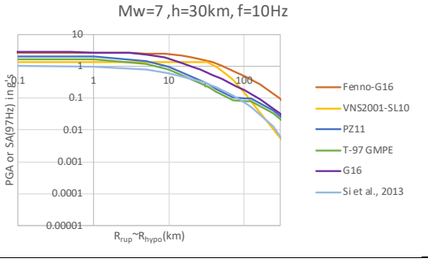	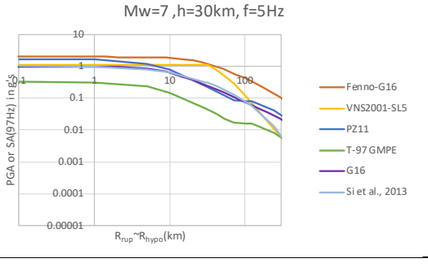	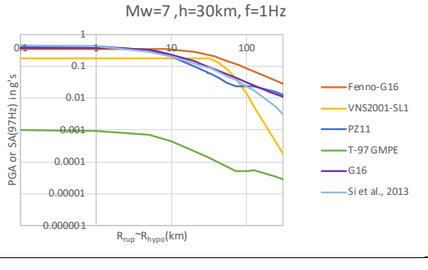

Annex B: Compare the Varpasuo Nikkari Saari / VNS (2017) components

	PGA	25Hz	10Hz	5Hz	1Hz
M_w=3	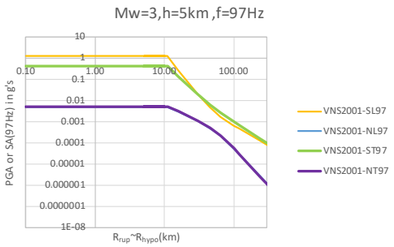	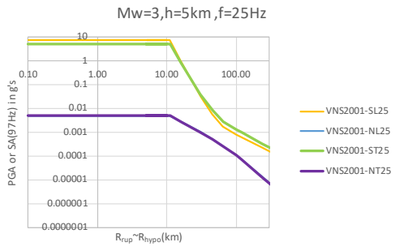	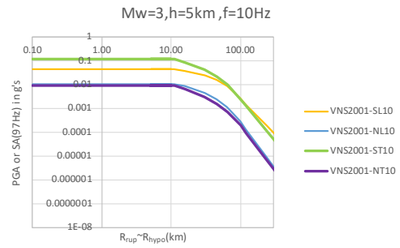	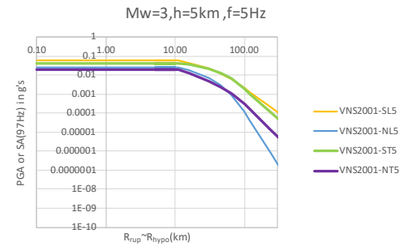	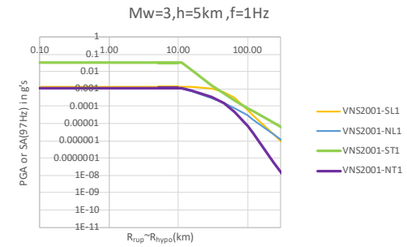
M_w=5	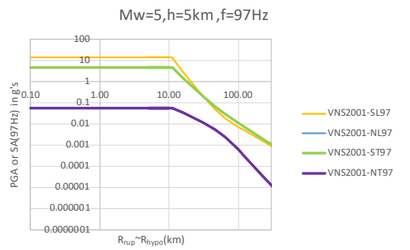	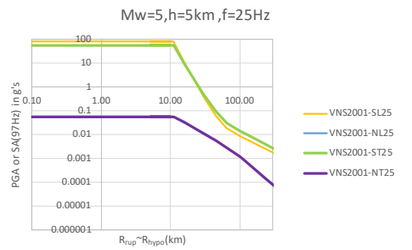	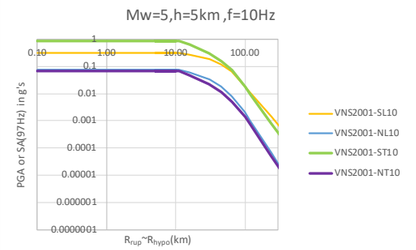	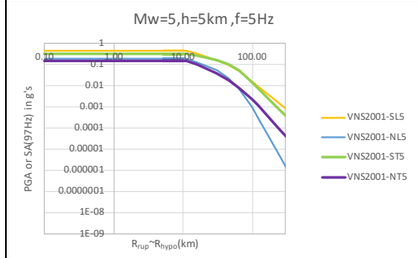	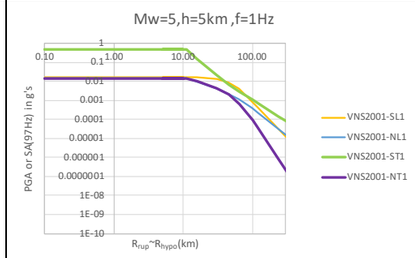
M_w=7	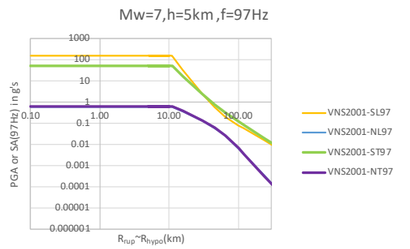	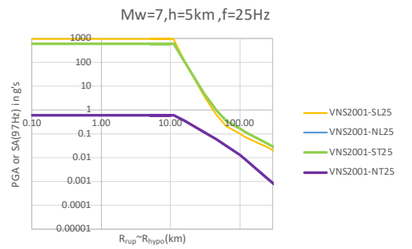	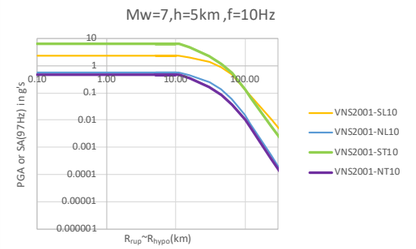	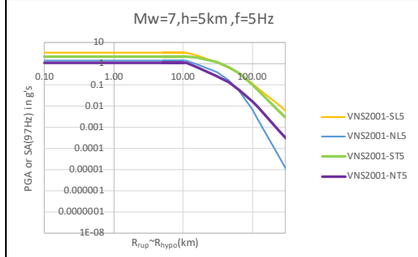	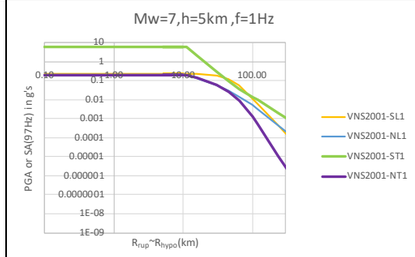
M_w=3	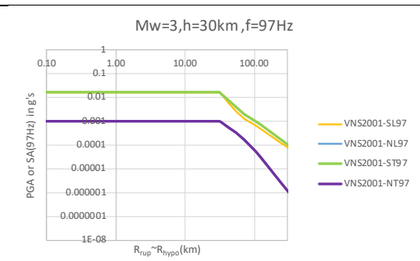	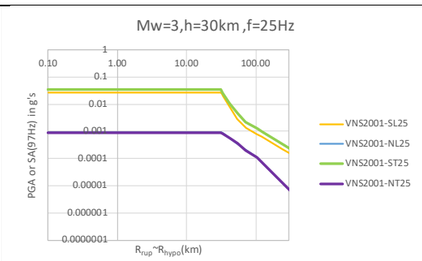	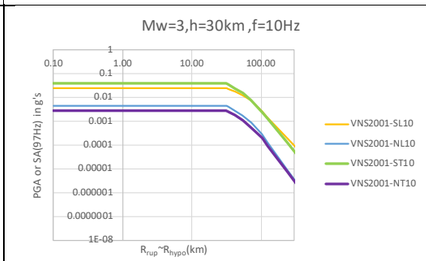	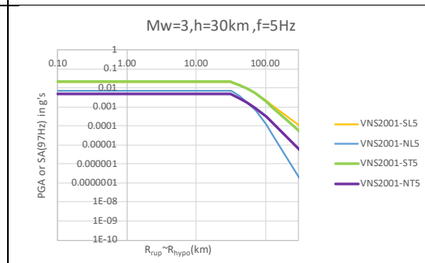	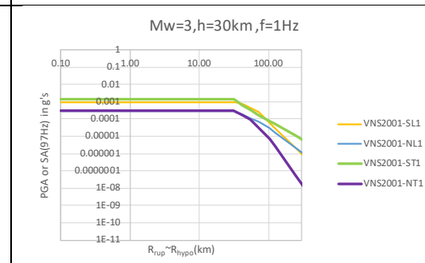
M_w=5	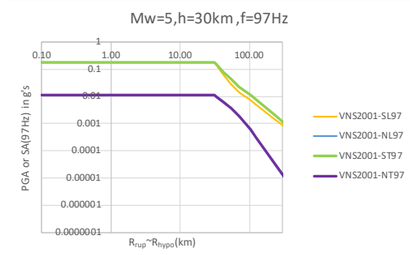	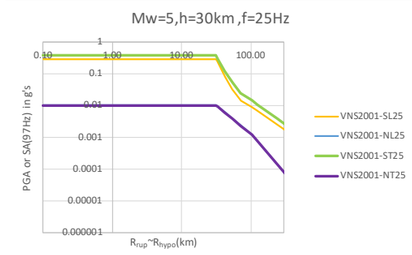	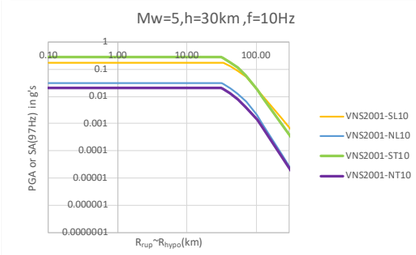	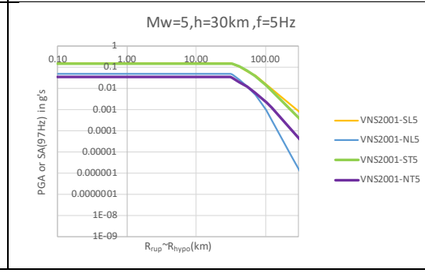	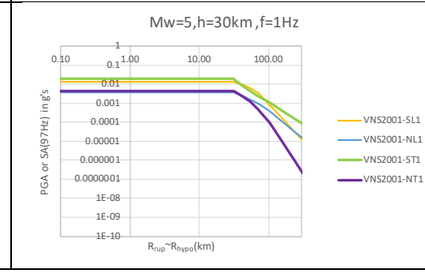

Appendix 3.7

M_w=7	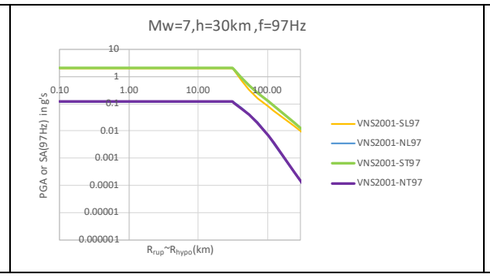	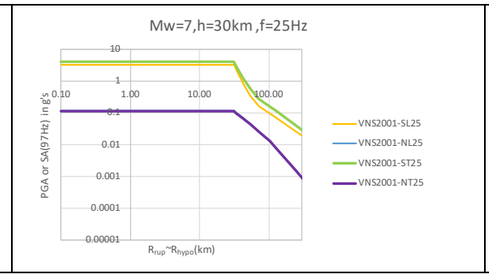	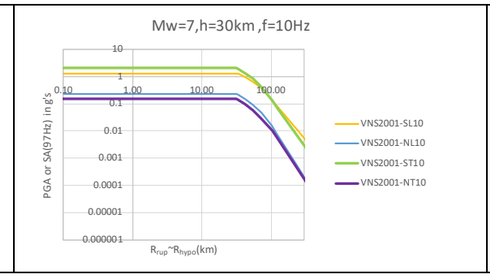	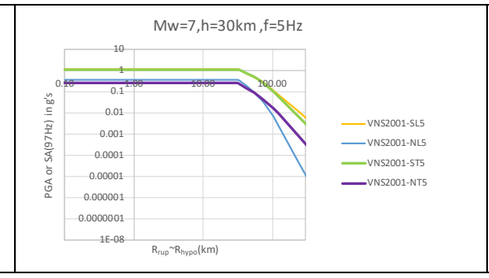	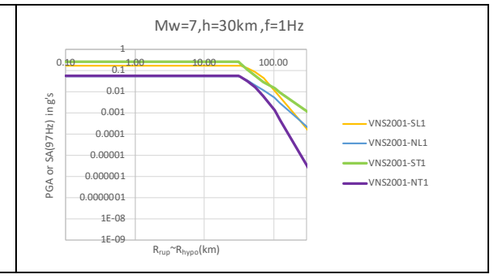

Annex C: G16 and Fenno-G16-to NGA East (only the range M_w4-7, which is common for all GMPEs – G16 is M_w4-8, Fenno-G16 is M_w2-7, NGA-East are M_w4-8.2)

	R_{rup}=5km	R_{rup}=20km	R_{rup}=50km	R_{rup}=100km	R_{rup}=200km	R_{rup}=300km
M_w=4	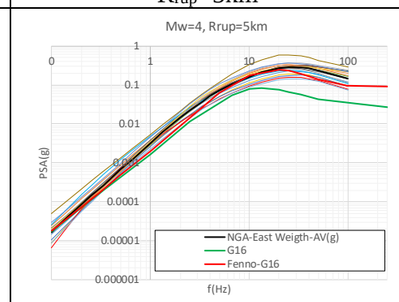	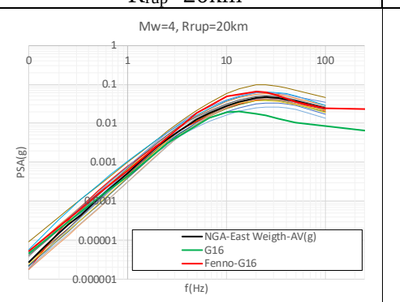	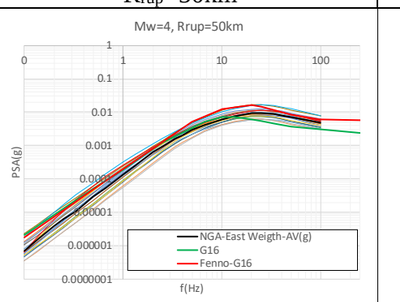	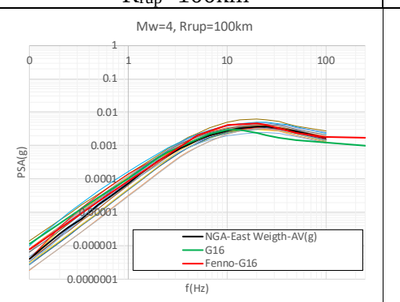	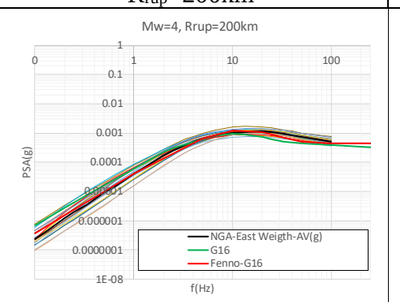	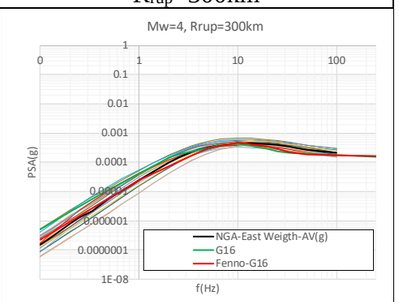
M_w=5	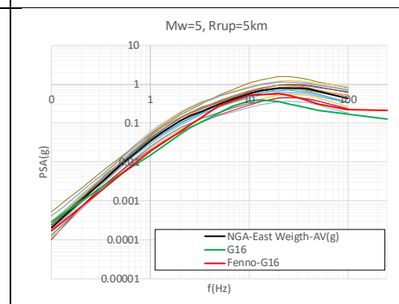	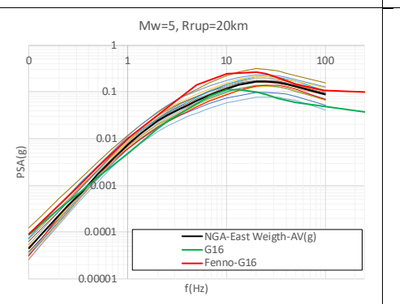	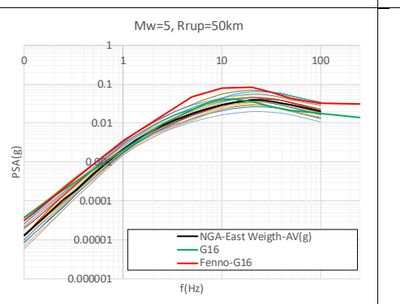	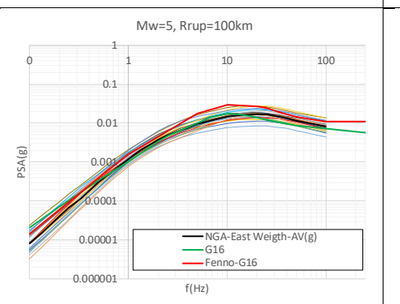	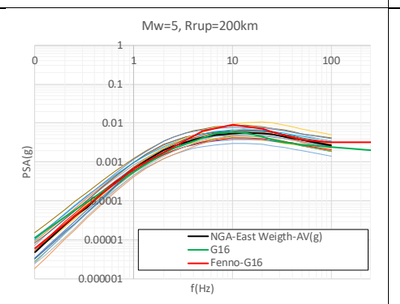	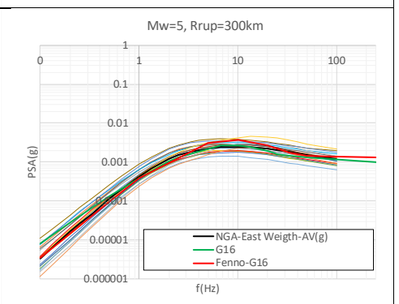
M_w=6	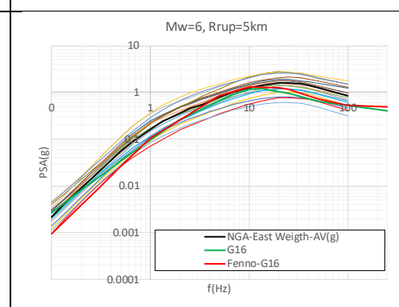	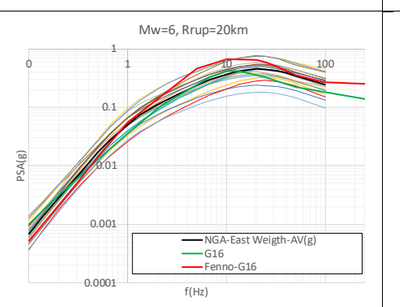	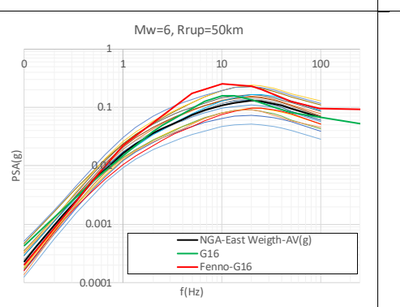	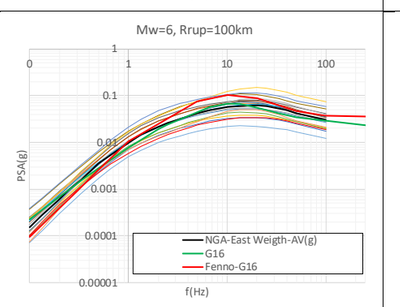	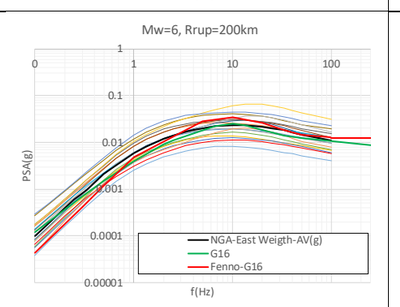	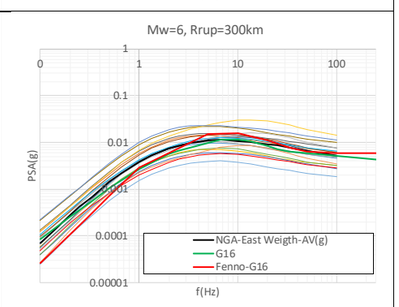
M_w=7	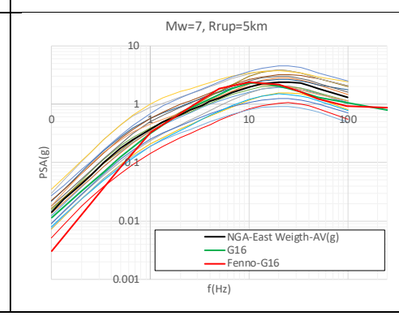	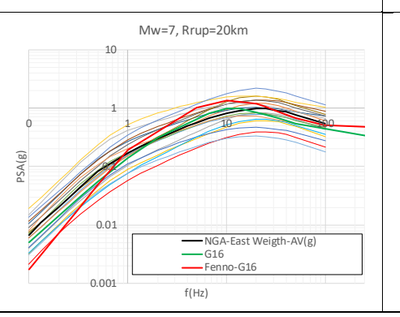	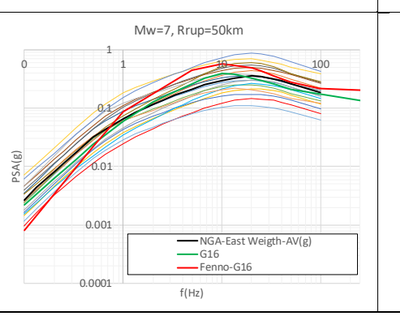	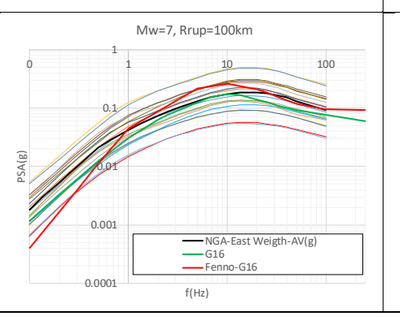	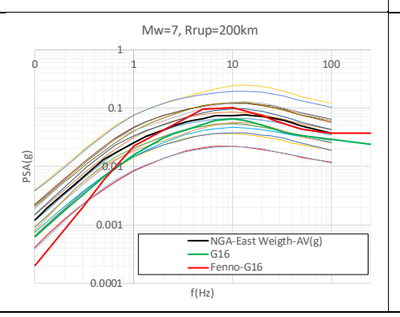	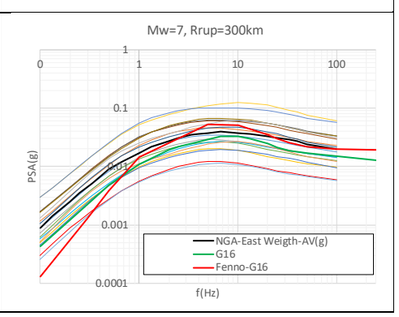

Annex D: Compare GMPEs_to_Data (T-97 is used in the Hanhikivi / update of the New Fennoscandian GMPES; some GMPEs are used outside their validity range

	PGA	25Hz	10Hz	5Hz	1Hz
M_w=2.4	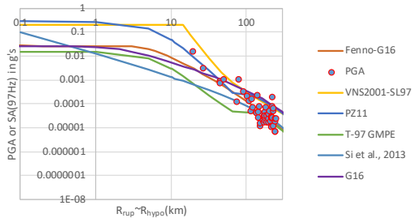	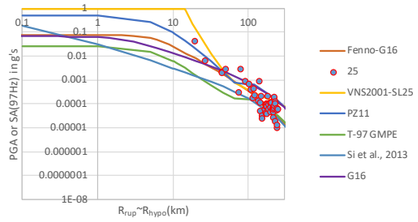	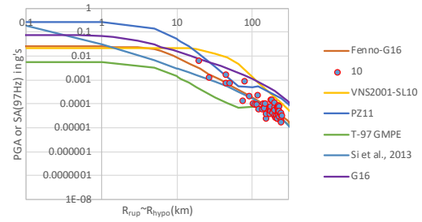	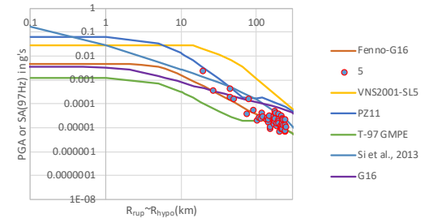	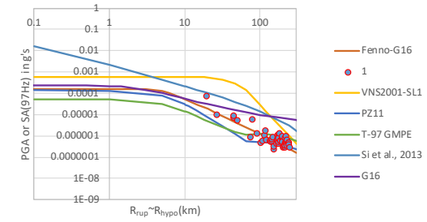
M_w=3.1	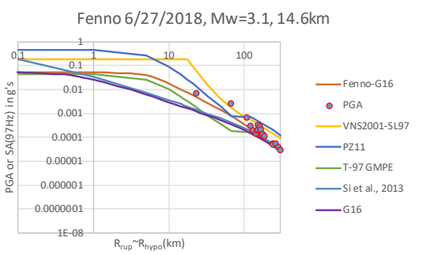	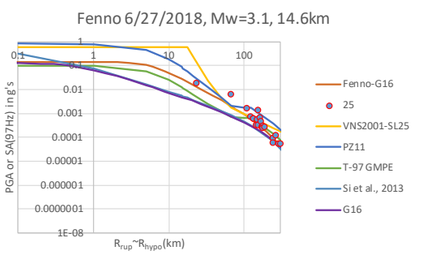	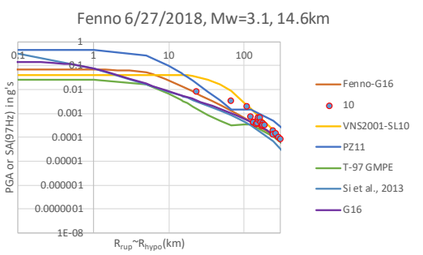	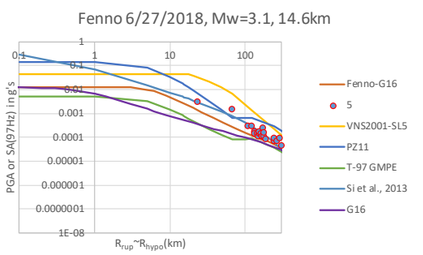	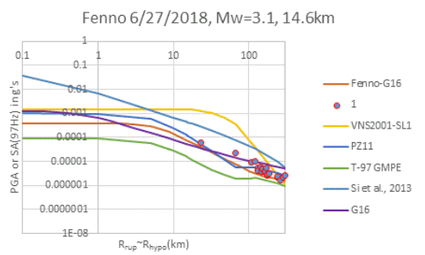
M_w=4.1	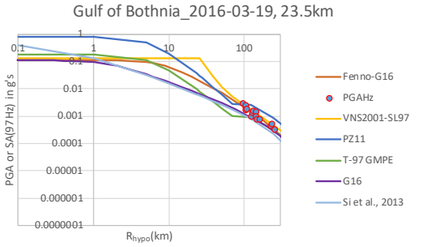	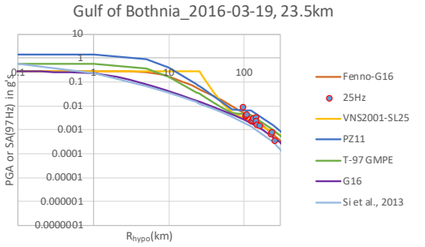	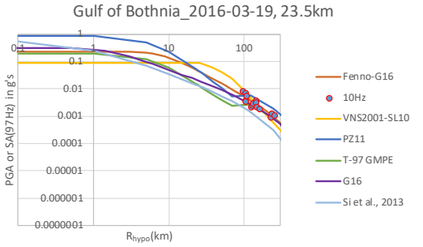	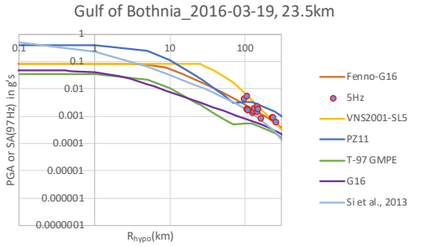	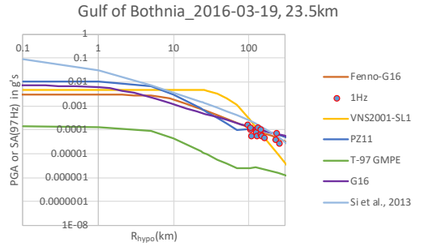
M_w=4.65	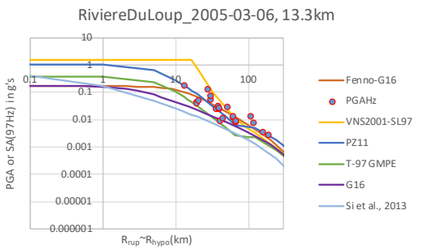	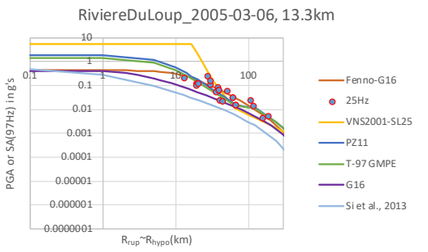	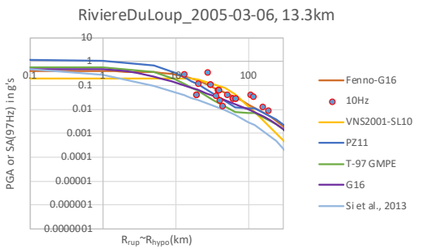	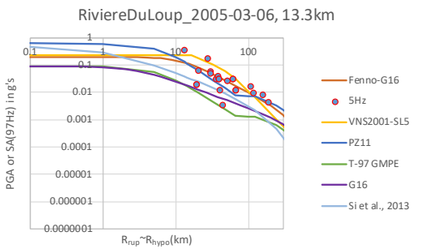	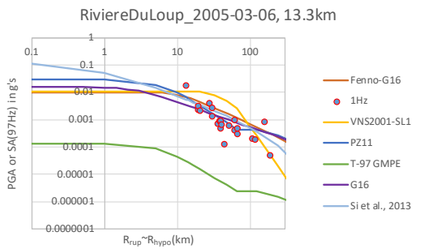
M_w=5.1	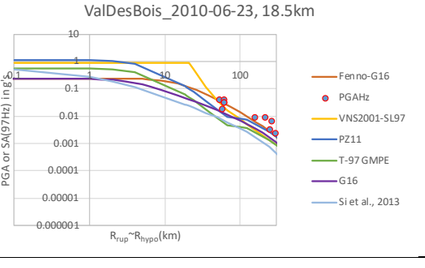	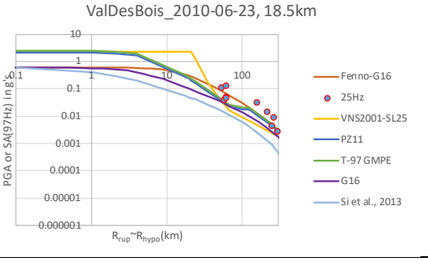	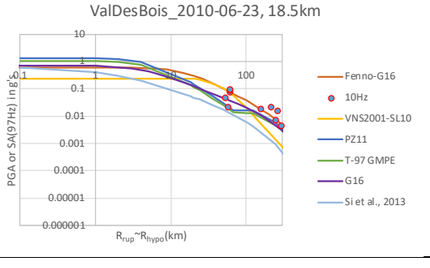	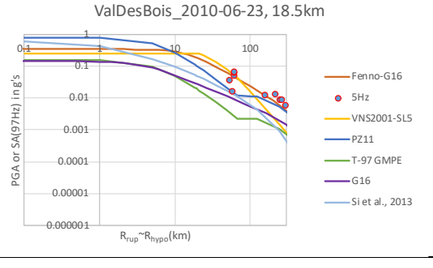	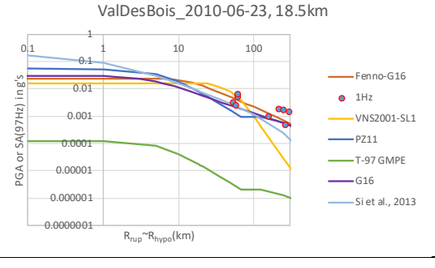

Appendix 3.7

M_w=5.85	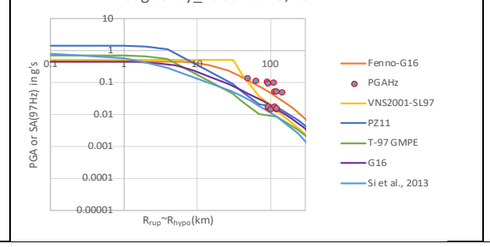	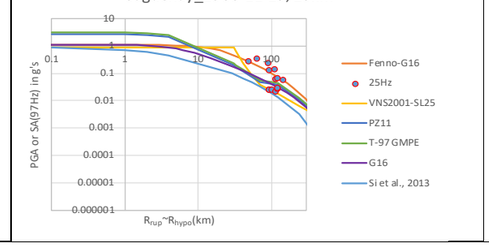	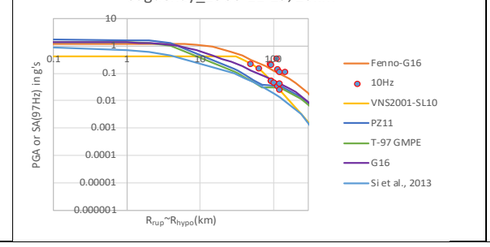	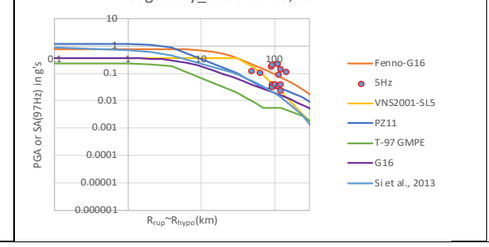	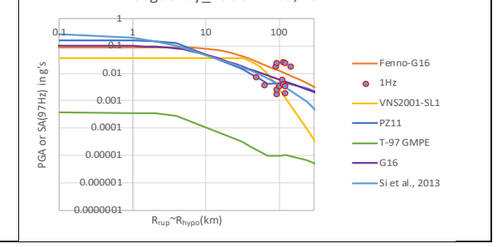

Annex E: Compare Varpasuo Nikkari Saari / VNS (2017) components to data

	PGA	25Hz	10Hz	5Hz	1Hz
M_w=2.4	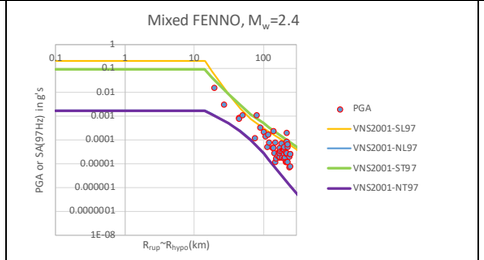	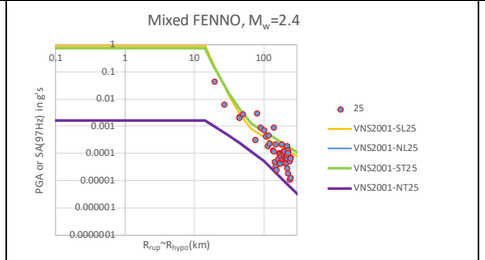	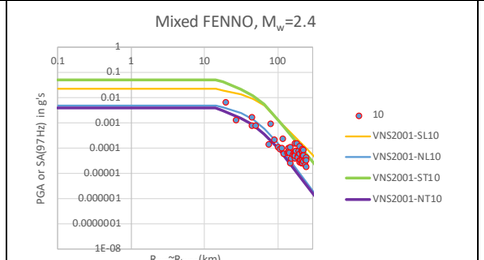	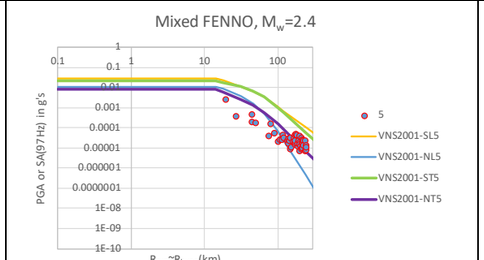	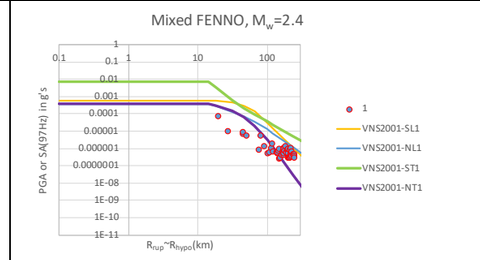
M_w=3.1	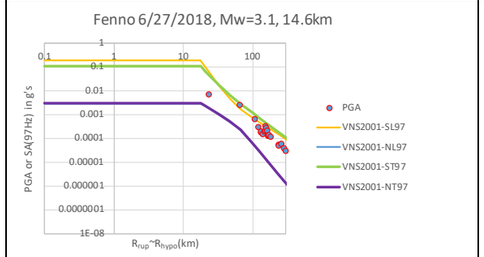	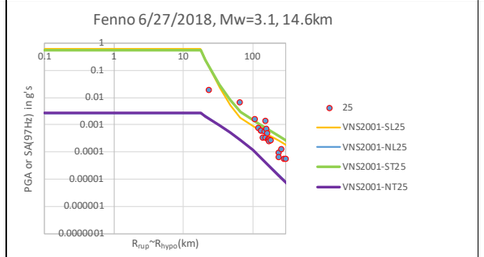	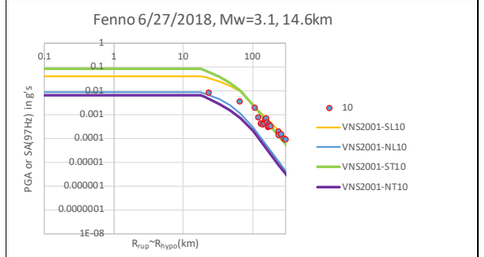	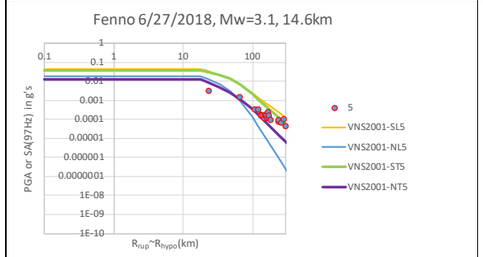	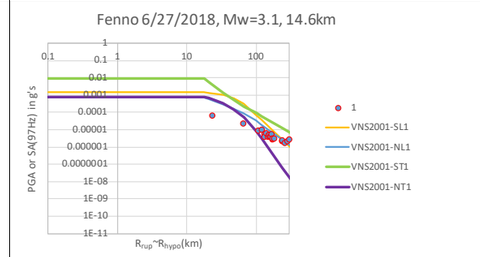
M_w=4.1	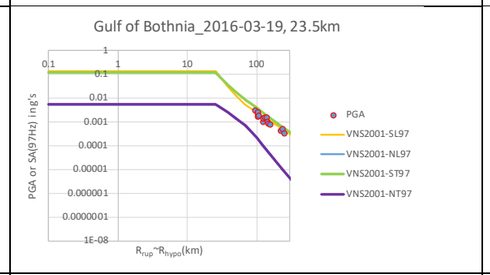	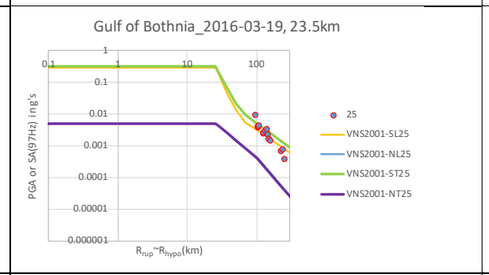	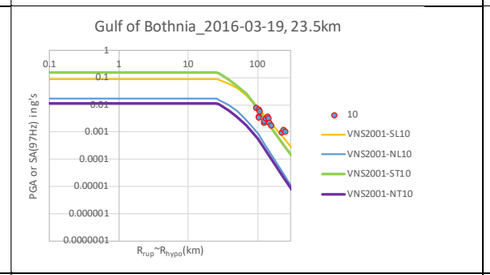	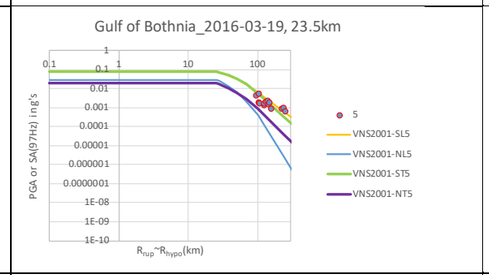	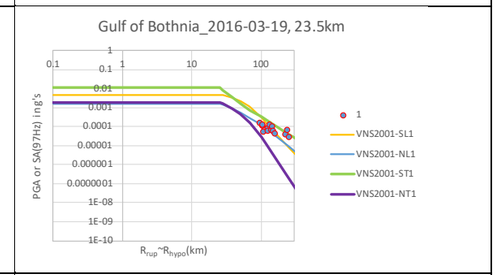
M_w=4.65	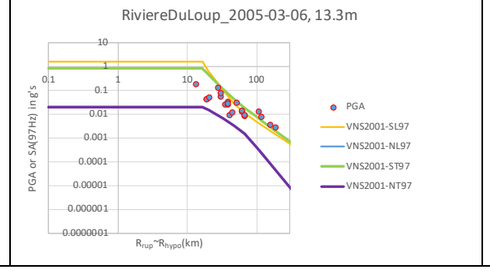	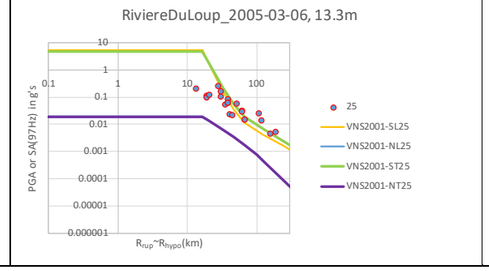	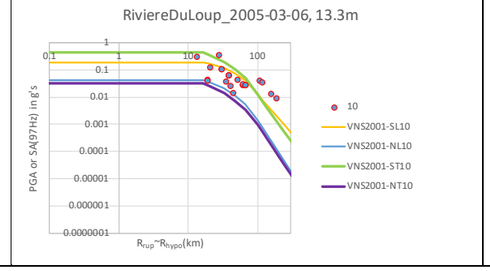	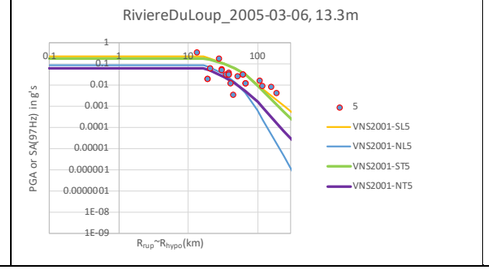	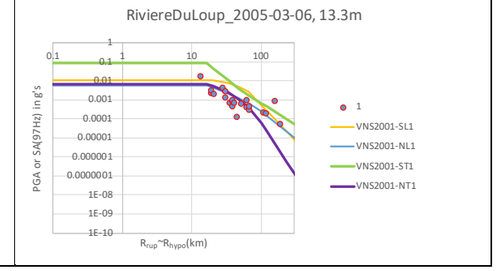

Appendix 3.7

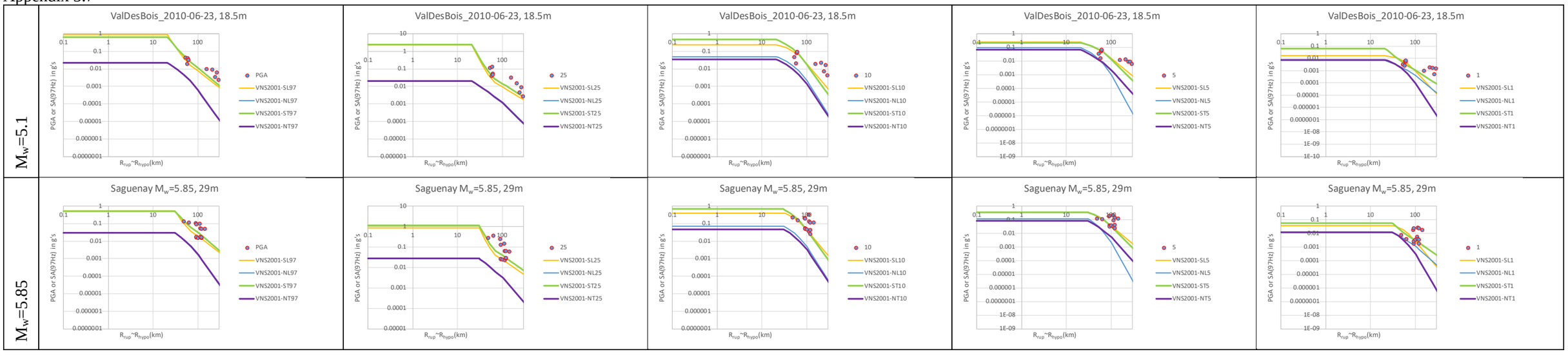
Mw=5.1
Mw=5.85
ValDesBois_2010-06-23, 18.5m
Saguenay Mw=5.85, 29m
PGA or SA(97Hz) in g's
Rrup~Rhypo(km)
PGA
VNS2001-SL97
VNS2001-NL97
VNS2001-ST97
VNS2001-NT97
25
VNS2001-SL25
VNS2001-NL25
VNS2001-ST25
VNS2001-NT25
10
VNS2001-SL10
VNS2001-NL10
VNS2001-ST10
VNS2001-NT10
5
VNS2001-SL5
VNS2001-NL5
VNS2001-ST5
VNS2001-NT5
1
VNS2001-SL1
VNS2001-NL1
VNS2001-ST1
VNS2001-NT1